

Electronic Theses and Dissertations, 2020-

2020

Additive Manufacturing of Elastomeric Lung Phantoms in Radiation Oncology

Jonathan Sookdeo
University of Central Florida

 Part of the [Mechanical Engineering Commons](#)
Find similar works at: <https://stars.library.ucf.edu/etd2020>
University of Central Florida Libraries <http://library.ucf.edu>

This Masters Thesis (Open Access) is brought to you for free and open access by STARS. It has been accepted for inclusion in Electronic Theses and Dissertations, 2020- by an authorized administrator of STARS. For more information, please contact STARS@ucf.edu.

STARS Citation

Sookdeo, Jonathan, "Additive Manufacturing of Elastomeric Lung Phantoms in Radiation Oncology" (2020). *Electronic Theses and Dissertations, 2020-*. 135.
<https://stars.library.ucf.edu/etd2020/135>

ADDITIVE MANUFACTURING OF ELASTOMERIC LUNG PHANTOMS IN RADIATION ONCOLOGY

by

JONATHAN SOOKDEO
B.S. University of Central Florida, 2017

A thesis submitted in partial fulfillment of the requirements
for the degree of Master of Science
in the Department of Mechanical and Aerospace Engineering
in the College of Engineering and Computer Science
at the University of Central Florida
Orlando, Florida

Spring Term
2020

Major Professor: Jihua Gou

ABSTRACT

Cancer is a particularly difficult disease to manage and treat, with cancer of the lung being a notably complex disease to treat with radiation therapy. In this study, a stereolithography-based 3D printing process was developed to fabricate human lung phantoms with identical mechanical and physical properties of human lungs in order to assist with targeted radiation therapy. A highly flexible UV photopolymer material with an elastic modulus of approximately 350 KPa was formulated for use in a custom-built stereolithography-based 3D printing apparatus. The printer built for 3D printing of the photopolymer features a large build volume with off-shelf components with fully open-source and efficient design. A lung phantom model of approximately 1/3rd scale was printed and further tested to simulate the tidal breathing motion in a respirator apparatus.

ACKNOWLEDGEMENTS

I would like to express my gratitude to Dr. Jihua Gou for accepting me into the Composite Materials & Structures Lab research group (CMSL), providing guidance for the duration of the program, and facilitating the development of this project and the machines required to produce results after a rapid change in the direction of the project.

I must extend my gratitude to Dr. Olusegun Ilegbusi and his former PhD student Dr. Don Nadun Kuruppumullage for their guidance and bridging the gaps of knowledge between the traditional mechanical engineering curriculum and the anatomy of the human lung.

I must also thank Dr. Kawai Kwok for extending his expertise in characterization of the material properties and testing of the polymer designed developed.

The aforementioned Dr. Jihua Gou, Dr. Olusegun Ilegbusi, and Dr. Kawaki Kwok should also be acknowledged for their assistance as part of the advisory committee formed for this thesis.

I would like to thank the industry sponsor of the project relevant to the thesis produced, CEO of SegAna LLC. Rodney Bosley—without whom the project would not have been possible.

TABLE OF CONTENTS

LIST OF FIGURES.....	vi
LIST OF TABLES.....	ix
LIST OF ABBREVIATIONS	x
INTRODUCTION.....	1
Motivation.....	1
Objective	1
Challenges	2
LITERATURE REVIEW	4
METHODOLOGY	15
Material Formulation	15
Machine Design.....	19
Frame.....	20
Substrate.....	26
Software.....	29
Model Preparation	31
TESTING AND EVALUATION	39
Early Stage Testing	39
Machine Print Testing	42

Manufacturing Challenges	49
CONCLUSION AND FUTURE WORK	52
In Summary of Work Completed.....	52
Future Work	53
Machine Design	53
Software and Processing	54
Material Design.....	56
REFERENCES	57

LIST OF FIGURES

Figure 1. Reference properties for materials cited in this work.....	5
Figure 2. Foam extrusion process.....	5
Figure 3. Early lung phantom respirator prototype.....	6
Figure 4. Ultimate design used to simulate respiration	7
Figure 5. Inflatable balloon printed with Ebecryl	8
Figure 6. A laser driven SLA (left) and DLP type SLA (right).....	10
Figure 7. Routed toolpath for a model with an FDM process	12
Figure 8. Routed toolpath for a model with a laser SLA process.....	13
Figure 9. Cross-section slice of the same model shown in fig. 7 and 8	14
Figure 10. Photoinitiator absorbance plots	18
Figure 11. Initial SLA-DLP machine concept	19
Figure 12. Substrate mounted to Z-axis platform subframe	21
Figure 13. Projector mounting hardware	21
Figure 14. TPU spacers on projector mounting points	22
Figure 15. Modular machine feet (black) with added press-fit extensions (gray)	24
Figure 16. Cross-section view of printer feet prepared for printing with high infill (85%) with 5 perimeter walls (left) and low infill setting (20%) with two perimeter walls.....	25
Figure 17. CAD model of final substrate design	27
Figure 18. Split portion of shaft	27
Figure 19. Upper portion of substrate	28
Figure 20. RAMPS 1.4 (left) and Arduino Mega 2560 (right).....	29

Figure 21. Full system hierarchy	30
Figure 22. Lung mesh after postprocessing (two perspectives)	31
Figure 23. Lung models prepped for printing	32
Figure 24. NanoDLP main interface	34
Figure 25. Ultimate print settings used	35
Figure 26. Collective figure of 9 discrete sequenced slices intended for SLA-DLP printing of a lung phantom.....	38
Figure 27. Deformation simulation strain response of real lung tissue (15 kPa)	40
Figure 28. Deformation simulation strain response of elastomer photopolymer formulation 5 of table 1 (300 kPa)	41
Figure 29. Provided legend for figures 27 and 28. Points 1, 2, 3, correspond to the top surface, inner surface near hilum, and bottom surface, respectively	41
Figure 30. First successfully 3D printed material sample	42
Figure 31. Diagram of bottom-up SLA machine.....	43
Figure 32. First SLA-DLP 3D printed sample	45
Figure 33. Late (left) vs early (right) print iteration samples.....	45
Figure 34. Original model of part shown in figure 33.	46
Figure 35. Final testing print at large volume.....	47
Figure 36. Late iteration lung phantom being printed	48
Figure 37. Final lung phantom print using custom resin formulation on custom designed SLA-DLP machine.....	49

Figure 38. 10 qt. vat with suspended custom developed UV photopolymer resin suspended, marked in red..... 50

Figure 39. Sample part with concave geometry..... 51

Figure 40. Alternate dissolvable platform 54

Figure 41. ML optimized cast provided by Stratasys 55

LIST OF TABLES

Table 1. Iterations of UV photopolymer resin intended for SLA-DLP 3D printing.....	16
--	----

LIST OF ABBREVIATIONS

ABS	Acrylonitrile Butadiene Styrene
BAPO	Phenylbis (2,4,6-trimethylbenzoyl)-phosphine oxide
CAD	Computer Assisted Design
DLP	Digital Light Processing
FDM	Fused Deposition Modeling
PETG	Polyethylene Terephthalate Glycol
PLA	Polylactic Acid
RAMPS	RepRap Arduino Mega Pololu Shield
SLA	Stereolithography Apparatus
STL	Standard Tessellation Language or Standard Triangle Language
TPO	Diphenyl (2,4,6-trimethylbenzoyl)-phosphine oxide
TPU	Thermoplastic Polyurethane
UV	Ultraviolet

INTRODUCTION

Motivation

Cardiovascular ailments remain as one of the major causes of death and remains a challenge to modern science. Malignant tumors, referred to as cancer, remains as a particularly difficult disease to manage and treat, with cancer of the lung being a notably complex disease to treat with radiation therapy. High energy or high dosage radiation waves are used in image guided radiation therapy, which is effective in killing cancer cells, but has the expected side effect of killing healthy lung tissue cells. Radiation exposure to healthy tissue is shown to increase mortality rate and decrease patient quality of life [1], so it is desirable to improve administration of radiation to an afflicted lung. The natural motion of the lung further complicates radiation therapy, as the motion must be compensated for in the treatment plan. Due to the deformable nature and unique anatomy of a given individual pair of lungs, treatment must be adaptable and highly specific to each patient to ensure minimal loss of healthy tissue.

Objective

The deformable lung phantom can mimic breathing patterns and characteristic motion of tissues to assist in radiation oncology treatment planning. The objective of this study is to develop and produce a deformable lung phantom intended to be used in optimization of radiation delivery on a patient-specific level.

4D (3D spatial + 1D temporal) materials and printing can be utilized to produce lung phantoms, which emulate a functioning diseased lung to improve patient radiological treatment. Note that “1D temporal” material designates a material intended to have a deformable and variable shape

as a function of time. Lung models can be generated and modified in tandem with a capable 3D printing apparatus and a specific material formulation to yield a model with acceptably similar properties and deformation to a disease lung. It is currently possible to map 4D imaging of a functional lung with a CFD model to replicate deformation with air flow [2]. A suitable elastomer resin mixture must be designed to produce structures which exhibit properties and behavior similar to a human lung. The elastomer resin mixture will be photopolymerized to build highly detailed and precise structures by means of SLA-DLP (digital light processing stereolithography apparatus) type additive manufacturing machine. The SLA-DLP machine will be application specific built to meet the requirement completing polymerization within a reasonable timeframe (24 hours) at a scale of $\frac{1}{4}$ minimum suitable for early stage testing. There does not currently exist a solution suitable for additive manufacturing of highly elastic photocurable polymer resins.

The manufactured lung phantom must be able to successfully simulate tidal motion in an artificial vacuum diaphragm. The lung must be air-tight and withstand an applied negative pressure across the outer surface. The respiration chamber will be provided and configured to a tidal volume of approximately $\frac{1}{3}$ rd scale of an adult human lung.

Challenges

This project had many limitations imposed on it to overcome. The most significant of which were circumstantial on the basis of time, budget, and material availability.

A previous team of students had worked in this project prior, the results of their work is similar to the content of this thesis, but from an alternative approach. Previous research was conducted on manufacturing of lung phantoms using foam extrusion and foam molding. Both foam

manufacturing techniques were found to be unable to meet the needs of the project sponsor and were abandoned to move in the direction of liquid resin polymers and SLA additive machines.

Consequently, a sizeable portion of the project budget and allotted time had been spent before the conception of this thesis, or any of the developments in it. As such, the project had to be completed in a such a way that minimized cost and favored rapid progress—this may help explain some of the design choices and standards used during the project detailed in this thesis.

Limited resources were available for machine design and printing parameters for the expected design. There was little reference material available for the liquid polymer resin configuration chosen. The lack of reference material in both core aspects of the design of the manufacturing process results in, metaphorically speaking, a system with many moving parts between integration of hardware, software, and materials.

An invaluable amount of time was saved by grace of luck that an entry-level consumer DLP projector with a short minimum focus length (<1.5 ft) and minimal UV-light filtering. These are both anomalies of consumer grade DLP projectors intended for media consumption in a home environment—typically UV light and short-range focus are undesirable and not necessary for the intended use.

LITERATURE REVIEW

The basis of DLP SLA 3D printing of phantom lungs for radiation therapy is predated as part of a capstone project by a group of students at University of Central Florida (UCF) to fulfill a portion of program requirements for a bachelor of science in mechanical engineering. The project was sponsored by SegAna and advised by Dr. Olusegun Ilegbusi of the mechanical and aerospace engineering department at UCF.

The final document produced by the group of students titled “Deformable Lung Phantom” provides a parallel framework with many shared goals, constraints, and ultimate purpose. The key deliverable of the cited project was used in performance evaluations of the produced lung phantom model using a custom-mixed polymer resin with an SLA-DLP additive manufacturing process. That is—the capstone project completed by the undergraduate students yielded a respirator device which simulates a human diaphragm with vacuum-driven inflation of the test apparatus (i.e. a lung phantom). The diaphragm prototype was tested with a lung phantom produced with a foam casting technique leveraging FDM (filament deposition modeling) additive manufacturing to fabricate a mold for the lung phantom. To repeat, the sole deliverable of the undergraduate project is the mechanical diaphragm used to mimic respiration—methods of phantom lung design, material, and fabrication were deliverables contained in the capstone project, but are to be considered obsolete and deprecated with regard to development on lung phantom fabrication. However, it is the preceding project which enabled to developments detailed within this thesis.

Between the completion of the previously mentioned “Deformable Lung Phantom Project,” some improvements were made to the fabrication process of lung phantoms manufactured using polymer foam molding but were found to be labor intensive and difficult to fabricate.

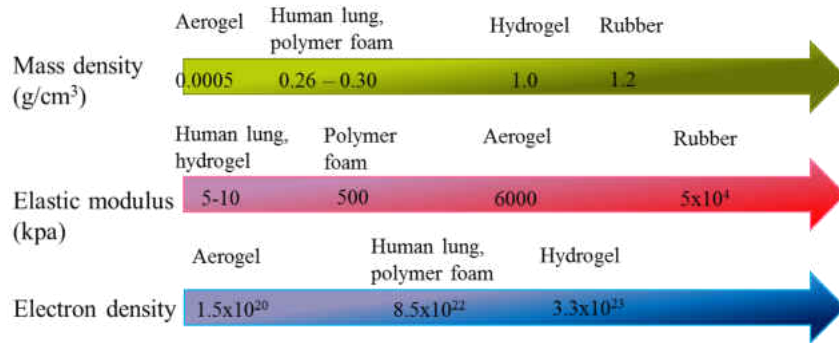


Figure 1. Reference properties for materials cited in this work

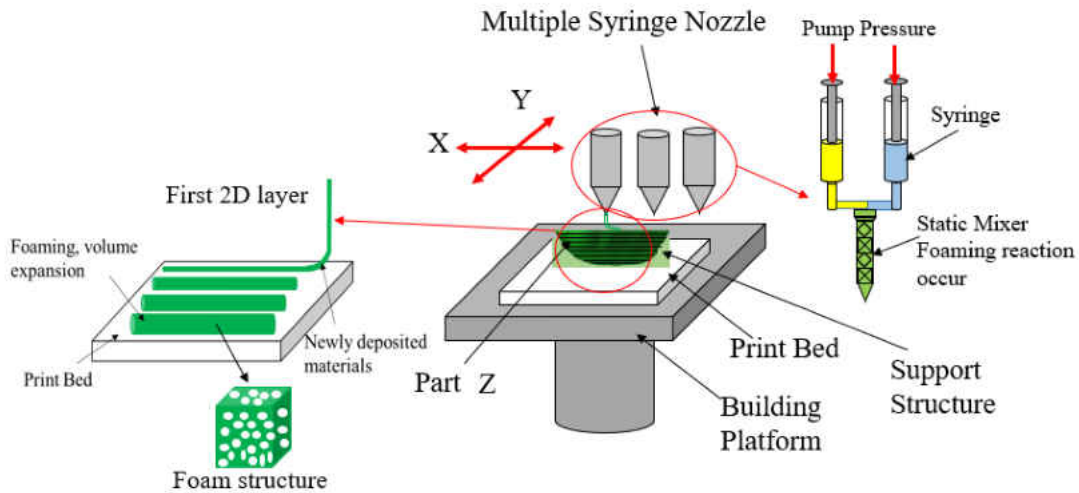


Figure 2. Foam extrusion process

Additional research was conducted attempting to print polyurethane foam based lung phantoms using a foam extrusion method with real-time mixing, but controlling extrusion and rate of cure was found to be far too complicated for the print quality achieved [3]

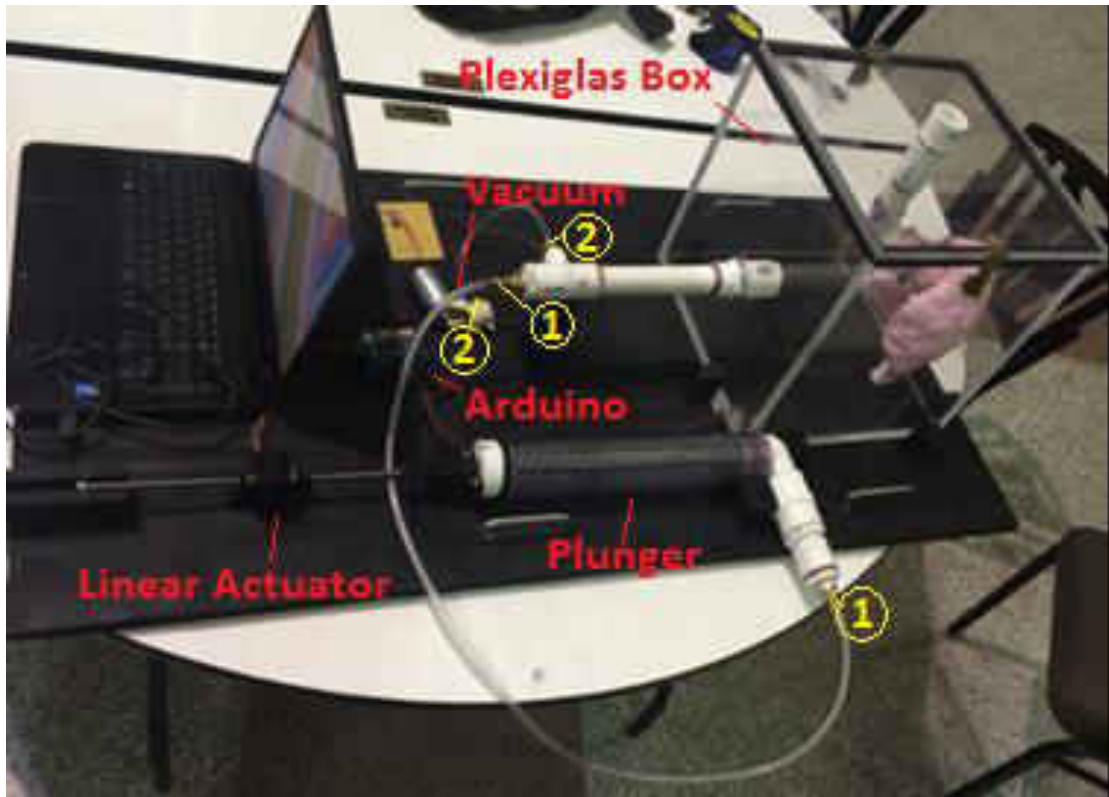


Figure 3. Early lung phantom respirator prototype

Figure 3. was taken directly from the report produced by the team of undergraduate students [4]. This prototype design was scaled up with increased specification to build a robust mechanical diaphragm.

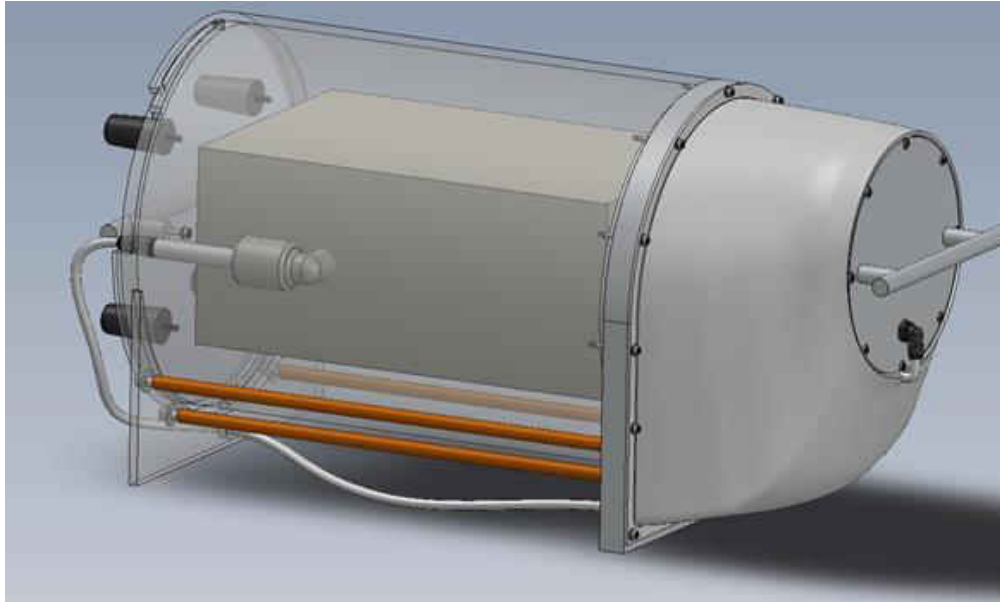


Figure 4. Ultimate design used to simulate respiration

The diaphragm shown in figure 4. was used with minor deviation from the depicted design to validate the lung phantom produced with an SLA-DLP additive manufacturing approach.

The findings of Patel et al. [5] with regards to highly stretchable UV curable elastomers have been the most impactful for the development of the lung phantom. The majority of the developments and content detailed in this work are based off and reference the findings of Patel et al. The materials investigated by Patel et al. are of particular interest, since there was a desire for UV curable resin materials with high elasticity to be used for additive manufacturing of lung phantoms. While multiple materials were analyzed by Patel et al., the select products 8413 and 113 of the Ebecryl product line from Allnex were found to have a peak elastic deformation of 1100%. The two-part mixture of Ebecryl products 8413 and 113 function as a difunctional oligomer crosslinker and monofunctional acrylated aliphatic epoxy reactive diluent, respectively. The two-part polymer mixture was varied from 0:10 (pure oligomer) to 5:5 (equal parts diluent

to oligomer); this yielded mechanical properties to be adjustable from 4.21 MPa and an elongation of approximately 1100% at 0:10 and 0.58 MPa with a maximum elongation of 240% at 5:5.

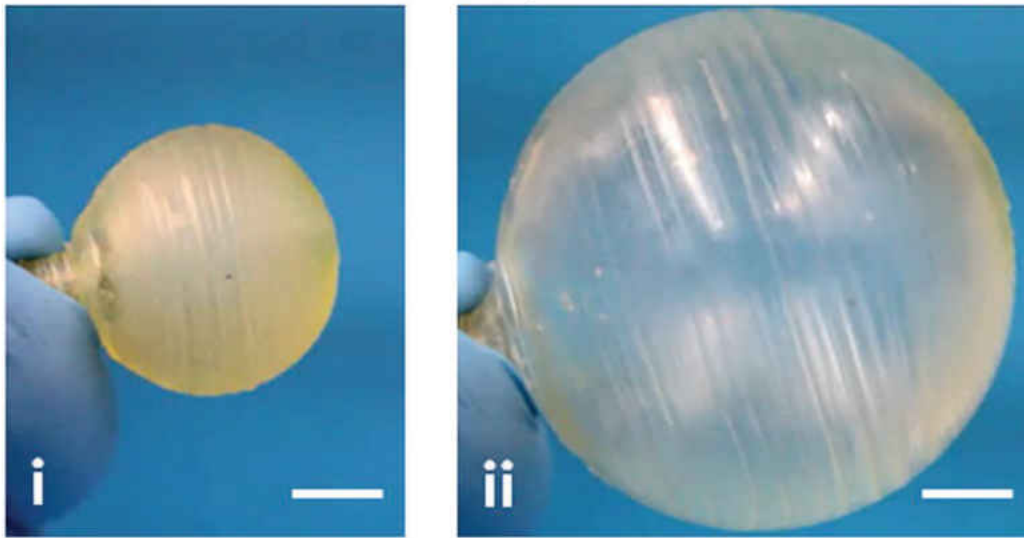


Figure 5. Inflatable balloon printed with Ebecryl

Patel et al. also demonstrated an analogous structure with SLA printed Ebecryl in the form of an inflatable balloon, which is reported to have been inflated to three times the original size. From the perspective of this project, this can be viewed as a rudimentary but functionally non-insignificant form of a lung.

Furthermore, while Patel et al. managed to loosely specify a material formula, Autodesk has publicly released a formula for an SLA compatible open-source resin system. As part of the (now defunct) Ember program, Autodesk shared a formulation for “PR48” [6] (prototyping resin 48th iteration) prototyping SLA resin optimized for highly detailed additive manufacturing by means of UV photopolymerization. The formulations given by Patel et al. and Autodesk were crucial

reference points for developing a resin suitable for SLA-DLP printing with the intention of producing a lung phantom.

As specified, Patel et al. provides a formulation of simply 2.00% wt. TPO (2,4,6-Trimethylbenzoyl-diphenylphosphineoxide) to any permutation of crosslinking oligomer to reactive diluent mixture. Autodesk formulation calls for Ebecryl 8210 (39.76%), Startomer SR494 (39.76%), Genomer 1122 (19.88%), TPO (0.40%), Mayzo OB+ (0.16%) wt., which function as oligomer, oligomer, reactive diluent, photoinitiator, and UV-blocker, respectively.

The resulting formulation used to fabricate a phantom lung based on the aforementioned consisted of 8:2 parts (vol.) Ebecryl 113 reactive diluent and Ebecryl 8413 oligomer, TPO (1.00% wt.), and Mayzo OB+ (0.10% wt.). The details of the chosen composition will be further elaborated on in chapter methodology.

The SLA additive manufacturing is the driving technology in fabrication of the lung phantom. SLA-DLP is used to produce lung phantoms, as such it is the process that is the most important to understand.

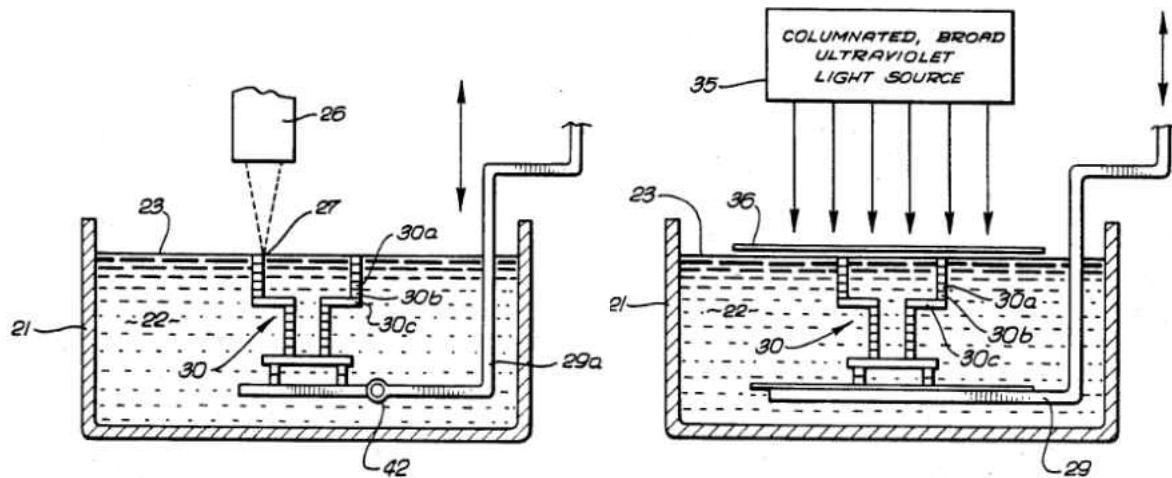


Figure 6. A laser driven SLA (left) and DLP type SLA (right)

The machine configurations shown in figure 6. were taken from the original patent for the technology filed by 3D systems in 1986 [7]. In process development for phantom lung production, an SLA-DLP machine was chosen for simplicity of design and construction—as a machine was required to be custom built to fit the needs of the project. The schematics shown in figure 4. are of very similar design and vary on by means photoinitiator activation, photopolymerization done with a galvo motor mirror system to direct the laser (typically 150-300mW) output is featured on the machine schematic on the left, and an SLA configuration using projected UV light is shown on the right.

Galvo motor mirror guided lasers trace paths into the substrate to polymerize a liquid resin layer by layer to fabricate a part—the laser path is treated as a toolhead and must be routed by controls software. The SLA-DLP method requires a digital projection device to project an image of a cross-section. Cross-sections can be generated in software; a model is partitioned into 2D sections of a designated thickness which correlates to the layer thickness of the fabricated model. Each individual cross-section is projected for a certain amount of time (typically 8-25 seconds)

onto the surface of liquid polymer contained in a vat. Once cross-section is cured, the platform which supports the part is moved downwards a specified distance (i.e. the layer height). The process of curing a cross-section and moving the platform downward is continued until the full body is fabricated. At the completion of the process, the part remains fully submerged and must be removed from the vat; while this requires a large volume of (often expensive) liquid resin, it allows the part to be printed fully supported and enables printing of complex geometries without consideration of gravity. The part is suspended during fabrication as the density after polymerization is practically identical to the liquid polymer resin.

It should be noted that thicker layers reduce the accuracy and quality of the part at the benefit of reduced printing time but require longer exposure time for digital projection-based SLA or the speed of the galvo-mirror system must be reduced to effectively increase exposure time. Optionally laser intensity may be increased, but this is not preferred due to degradation in print quality. Exposure in this context refers to the amount of UV light exposed to the material—sufficient UV exposure is required to fully activate the photoinitiator (TPO) and increasing layer thickness requires a greater amount of energy imparted for complete polymerization at finite volume scale.

While there are benefits to each technique, galvo-laser type SLA requires far more complex control and calibration. SLA-DLP can be quickly built with off the shelf components, is faster to calibrate, easy to expand, and faster for fabricating larger objects. The speed advantage in SLA-DLP is given by the fact that scaling an object to be fabricated results in a linear increase in print time, whereas scaling objects for galvo-laser type SLA is a cubic increase in print time; this is on account of print time scaling solely with Z-direction (up and down) as changes in cross-sectional

area is time-static since the light projection device is always held at constant exposure time. Further clarification may be found in the machine design section should this concept remain unclear.

A very brief overview of the parallels between FDM may help explain galvo-laser type SLA printing. Traditional FDM, or molten polymer extrusion to construct an object is driven by the same kinematics and nearly identical controls. Many galvo-laser SLA machines can be driven with the same software as used in FDM, but with different machine parameters. The focal point of the laser can be treated in the same manner as the toolhead of an FDM machine where the software must route a path for a toolhead the size of the laser point.

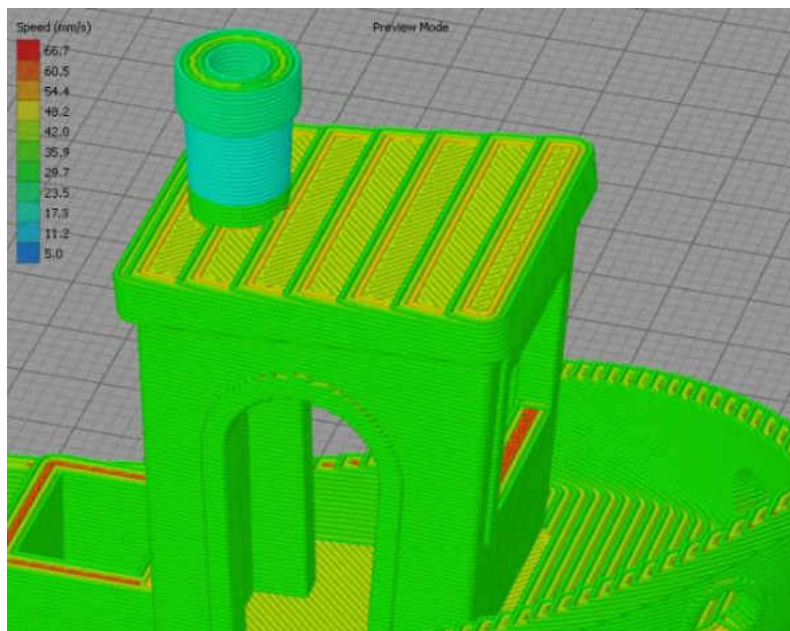


Figure 7. Routed toolpath for a model with an FDM process

Toolhead paths are outlined in figure 7. for a part fabricated by an FDM process. The traces shown in the figure 7 were routed under the assumption of a 0.4mm extrusion nozzle with a 0.3mm layer height. Layers can be similar for a galvo-laser SLA process should the layer heights be

equivalent—however differences in path outlines will be evident and due to the differences in effective diameter of the FDM extrusion head and the laser beam.

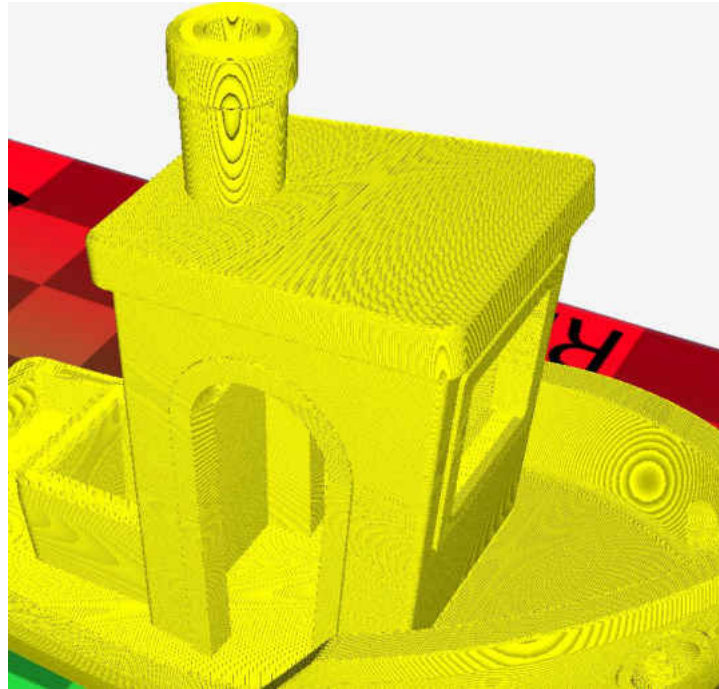


Figure 8. Routed toolpath for a model with a laser SLA process

The toolhead path in figure 8 can be compared to the path shown in figure 7. The models used are identical, and the software used to generate these paths are functionally equivalent. The laser “nozzle” or spot size used was 0.067mm with a 0.05mm layer height. The only differences between the models are print settings, as features used in FDM processes can be disabled or are analogously usable for a laser driven SLA process.

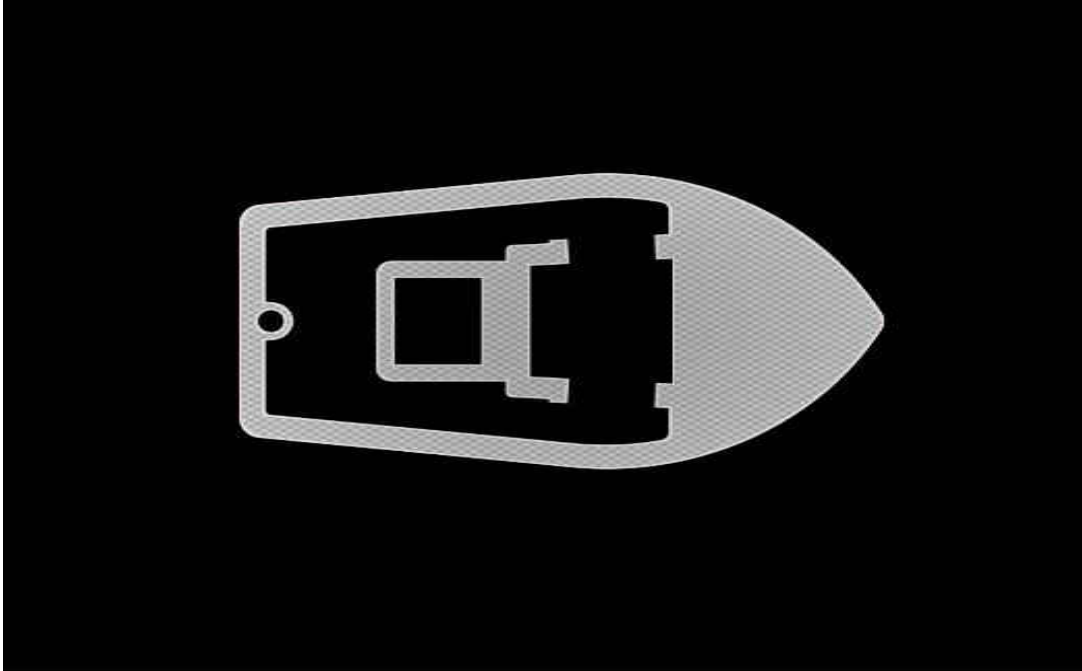


Figure 9. Cross-section slice of the same model shown in fig. 7 and 8

For comparison, figure 9. is what could be expected from an arbitrary cross-sectional layer projected onto the surface of the liquid polymer resin contained in a vat for a SLA-DLP 3D printing process. The area with a hatched shading is intended to be polymerized and fully cured, whereas the regions shown as black are expected to receive insignificant amounts of UV exposure and remain in liquid polymer resin state. Identical models of a miniature boat were used to generate the toolpath in figure 7, 8 and the cross-section in figure 9.

METHODOLOGY

Material Formulation

The reactive diluent Ebecryl 113 and crosslinking oligomer Ebecryl 8413 were tested at various ratios from 2:8 to 9:1 by volume. It was found at a 9:1 ratio of reactive diluent to crosslinking oligomer that polymerization became unstable and the material would never fully cure under directly under a UV light source. This indicates that the limit for the reactive diluent is between 8 to 9 parts to achieve complete polymerization with minimal crosslinked polymer network formation. A low crosslinking density is desirable for use in fabrication of lung phantoms to maintain a low modulus of elasticity at the expense of decreased allowable maximum elongation.

During early feasibility evaluation of the material, a non-rigorous test of the material was performed by the Structures and Material Design lab, directed by Dr. Kawai Kwok. A test strip of 20x40x100mm was used to determine a modulus of elasticity of approximately 300 kPa. A modulus of elasticity in the range of 250-400 kPa is approximately one order above the modulus of elasticity of human lung tissue (1-15 kPa surveyed from multiple sources)[8][9] but deemed to be acceptable as the difference in elasticity can be accounted for by increasing the applied pressure in the respirator apparatus.

Ultimate custom material formulation was derived by trial and error experimentation with later inspiration from Autodesk PR48 formulation. A set of formulations and a summary of the effect of varied parameters is presented in table.

Table 1. Iterations of UV photopolymer resin intended for SLA-DLP 3D printing

<u>Composition</u>	<u>Ebecryl 113:8413</u>	<u>Photoinitiator</u>	<u>Photoinhibitor</u>	<u>Observations</u>
1	5:5	BAPO – 2% wt.		Successfully cured material under UV-light, initially chosen due to strong absorption in 360-410nm spectrum. Material is flexible, but still too rigid for application.
2	5:5	TPO – 2% wt.		Switched photoinitiator to TPO, while less effective produces a fully transparent body compared to the yellow tint of BAPO. First successful print in bottom-up laser driven SLA consumer printer (Peopoly Moai)
3	8:2	TPO – 2% wt.		Successful cure of first sample batch at 8:2 ratio of monofunctional reactive diluent to crosslinking oligomer. Modulus later found to be approximately 350kPa with MTS tensile testing machine.
4	9:1	TPO – 2% wt.		First unsuccessful attempt at curing under direct UV light source. Material failed to form homogenous fully crosslinked elastomer given ample time under direct UV light source. Maximum diluent to oligomer ratio for successful cure determined to be between 8:2 and 9:1.
5	8:2	TPO – 2% wt.		Complete polymerization under UV light source. Material fails under bottom-up laser driven SLA printers due to highly elastic materials being intrinsically incompatible with bottom-up designs
6	8:2	TPO – 1% wt.		Reduced excess photoinitiator to yield more efficient formulation. Tested successful on small scale with first iteration of top-down SLA-DLP machine.

<u>Composition</u>	<u>Ebecryl 113:8413</u>	<u>Photoinitiator</u>	<u>Photoinhibitor</u>	<u>Observations</u>
7	8:2	TPO – 1% wt.	Azo/Rit dye	Dark color dyes added to control depth of free radical polymerization and reduce over-cure from light diffraction. Severely impeded polymerization, likely too much dye added. Could possibly compensate by increasing UV-light exposure time, but this is an extremely inefficient and impractical solution.
8	8:2	TPO – 1% wt.	Benetex OB plus – 0.05%	Successful cure with little to no effect on cure times. Printed model fully polymerized.
9	8:2	TPO – 1% wt.	Benetex OB plus – 0.1%	Successful cure with mild effect on cure time, but much higher detail and control over polymerization. Formulation deemed acceptable, further optimization is possible, prevented by limited material availability
10	8:2	TPO – 1% wt.	Benetex OB plus – 0.1%	Glycerin added to greatly improve process efficiency. Photopolymer mixture is suspended on glycerin in a liquid vat enable large build volumes while only requiring a fraction of photopolymer material. Only a thin layer of liquid photopolymer is required on the surface to produce a solid body.
11	8:2	TPO – 1% wt.	Benetex OB plus – 0.1%	SLA-DLP machine upscaled to accommodate 10 qt. build vat. Allowable build dimensions of approximately 8 in. diametral and 8 in. depth. Thin layer of liquid photopolymer is floated on glycerin, allowing large parts to be printed.

Some iterations tabulated were tested multiple times with slightly varied print settings simultaneously. This was done in cases of failure or if minor setting changes were speculated to benefit print quality.

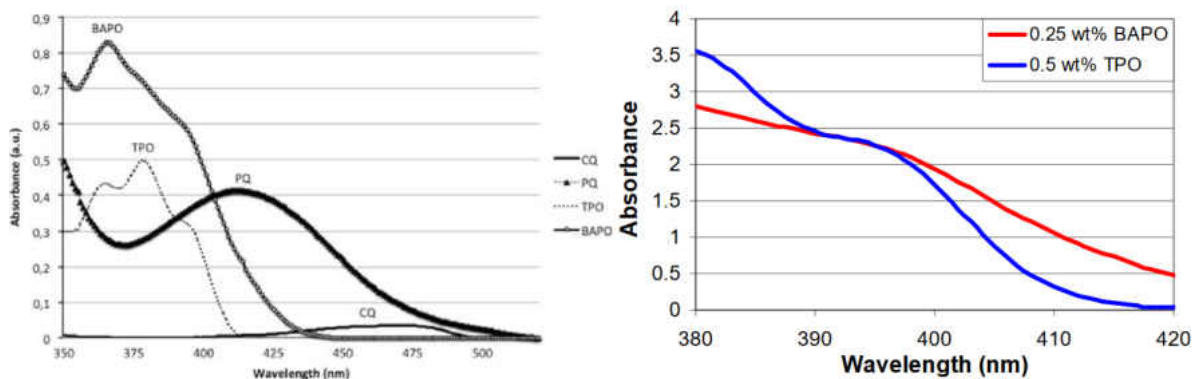


Figure 10. Photoinitiator absorbance plots

Figure 10 plots contain photoinitiator BAPO versus TPO [10], suggesting that roughly half the amount by weight of BAPO is functionally equivalent to TPO in terms of UV absorbance, provided in support of Table 1. Camphorquinone was also tested before using phosphine oxides BAPO or TPO, but as the plot suggests has very low absorbance and reduces optical properties by functioning as a yellow colorant.

Machine Design

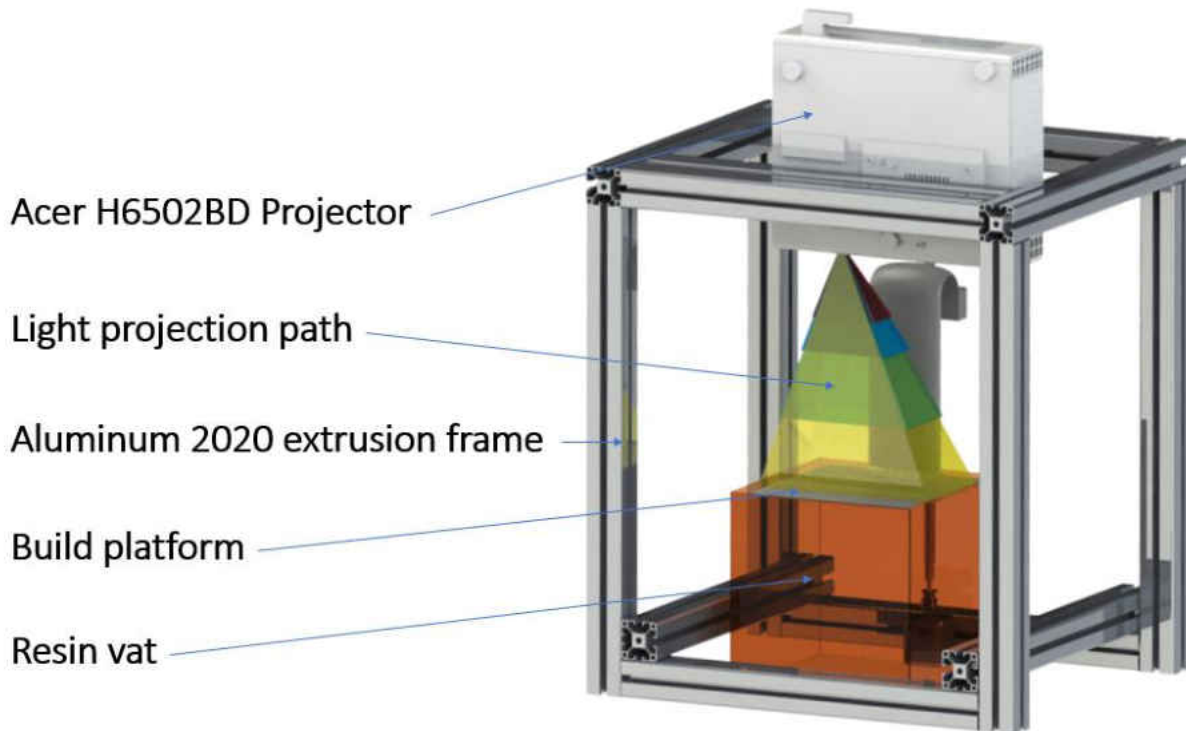


Figure 11. Initial SLA-DLP machine concept

The sketch shown in figure 11 was the expected design for the top-down SLA machine. Actual machine construction closely followed the sketch, with primary differences in implementation being the build substrate and Z-axis apparatus. An Acer H6520BD DLP projector was selected as a broad-spectrum light source, which happens to have sufficient light output in the sub-450nm ultraviolet range to allow free radical polymerization with a selected UV photoinitiator. The expected constructed was planned in such a way to enable a highly adjustable and flaw tolerant design, featuring as much 3D printed components as possible to enable rapid machine iterations and greatly reduce overhead. This allows significant design revisions to be performed on a practically nightly timeline if needed, as the lab group has multiple machines that can be used to fabricate new components simultaneously.

Primary design factors follow:

1. Adaptability
2. Construction speed
3. Scalability
4. Cost-effectiveness
5. Off-shelf components

To which, this machine design closely follows this guideline and priorities. Components were intended to have short lifecycles and mostly disposable to reduce as many restrictions and obstructions on future modifications.

Frame

The frame was constructed with 2020 aluminum T-slot extrusions, interlocked with T-nuts and 90-degree cast aluminum corner brackets ensure high rigidity. Aluminum extrusions are easily accessible, inexpensive, easy to machine, and implicitly creates a modular design. At a glance, 2020 extrusions may seem underwhelming for a 3D printer, but this machine bears no substantial loads, has negligible concern with vibrations, and will have negligible jerk from motion in the Z-axis.

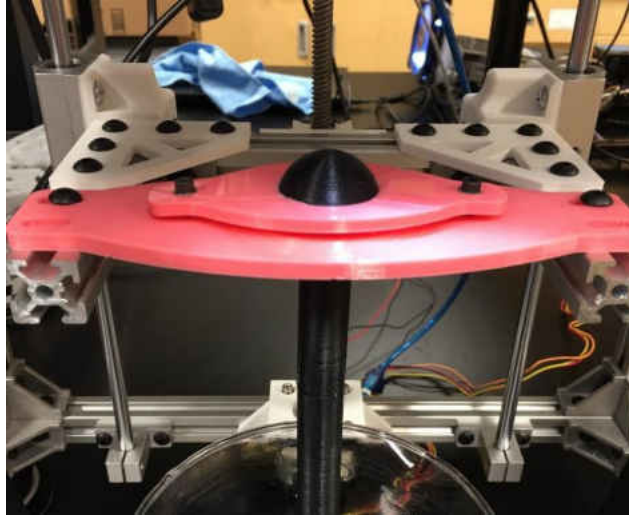


Figure 12. Substrate mounted to Z-axis platform subframe

3D printed parts were used in locations where rigidity is not critical and loading conditions are mild, with a notable exception shown in figure 13. White corner brackets shown in figure 12 were used as supplementary hardware to the cast aluminum corner brackets—this was done to reduce torsion across the member by uneven moments induced by the substrate mount.

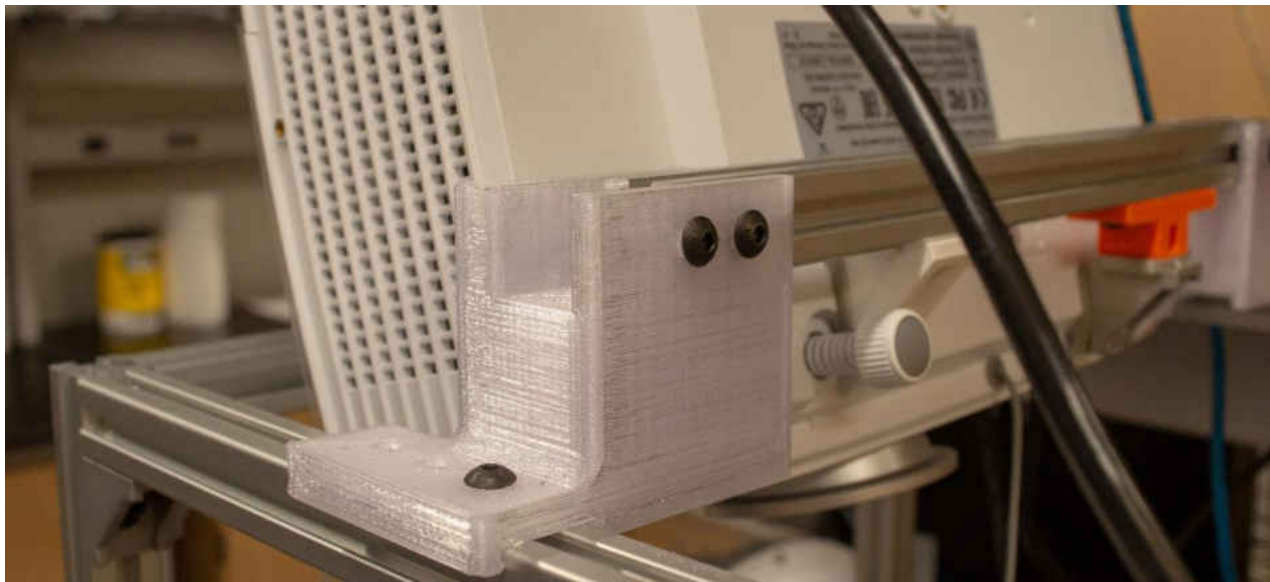


Figure 13. Projector mounting hardware

The projector mount is likely the largest load-bearing component on the machine, as well as the component with the most critical failure. The semi-transparent colored components shown in figure 13 were substantially overbuilt and printed with PETG at high infill density. Following the design philosophy of the machine, the mounting bracket was also a component that could be expanded vertically to increase the minimum focus height of the machine (i.e. raise projector elevation to enable a taller substrate, effectively increasing build volume with no required changes to the rest of the frame).

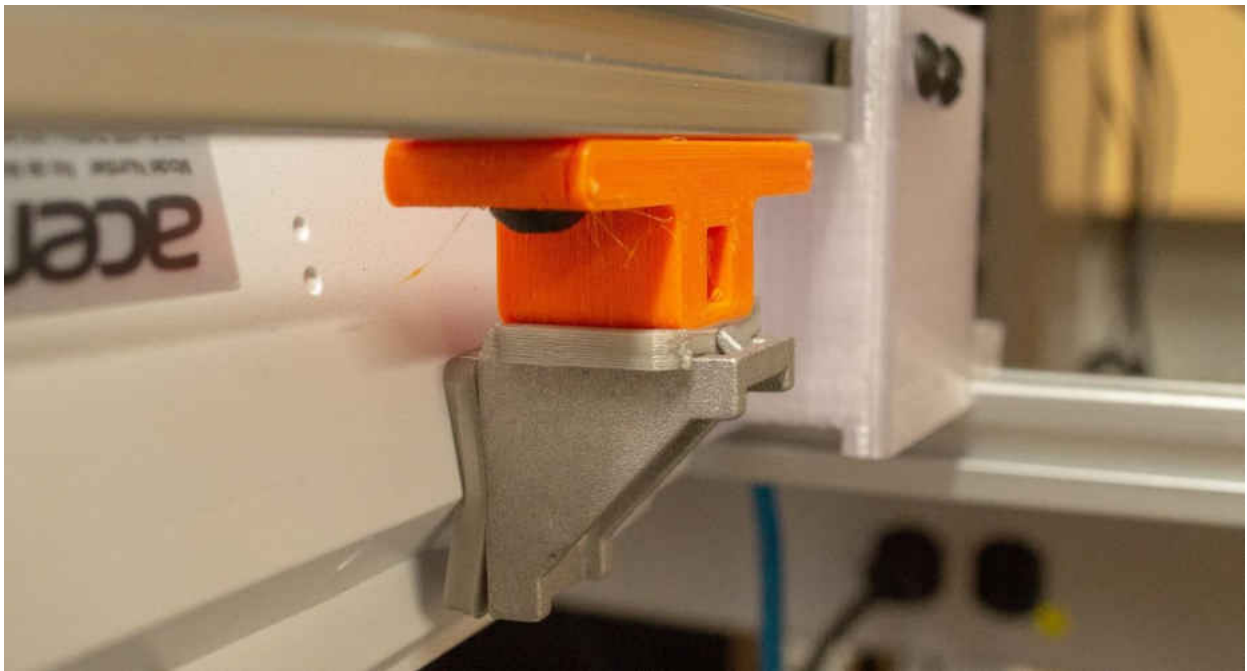


Figure 14. TPU spacers on projector mounting points

Thermoplastic polyurethane (TPU) was used on mounting points between the machine frame and the projector. These spacers shown in figure 14 behave as small spring dampers, increase impact strength, and prevent brittle failure should the machine be subject to any sudden shock. The reduction in rigidity at this joint is worth added reliability.

An important but less obvious aspect of design are the print settings used to manufacture components of the machine. For load-bearing parts it is advisable to use a high percentage of infill coupled with a high count of exterior part walls to maximize part strength. In theory, a part of 100% infill should yield the best performing part, and in practice this is mostly true but also vacuous. Unless the component is intended to function until failure (i.e. high load-bearing non-critical component) it is not an efficient use of material or time. Often producing a part at 100% infill may also negatively impact print quality due to slight variances in material extrusion rates. Material extrusion rate has small fluctuations due to variance in diameter filament sold as consumer FDM 3D printing media. Voids in printed parts with less than 100% infill can function as buffer regions for excess material flow—this is a particularly important means to cope with excess material extrusion which may occur while the print head is idle during the transition between layers.

There are additional optimizations that can be done for printed parts that are subjected to uniaxial loads orthogonal to the (printing) XY-plane, specifically compressive loads. Traditional FDM 3D printed parts will always have anisotropic material properties, with the highest ultimate strength in compressive loads and weakest ultimate strength orthogonal to the XY-plane. Low tensile strength in the Z-direction (relative to the machine) is caused by the material behaving similar to a laminated composite material where failure by delamination across a plane parallel to layer orientation is the primary mode of failure under tension. For components such as the feet of the machine shown in figure 15, a lower infill setting can be selected without compromising compressive loading ultimate strength.

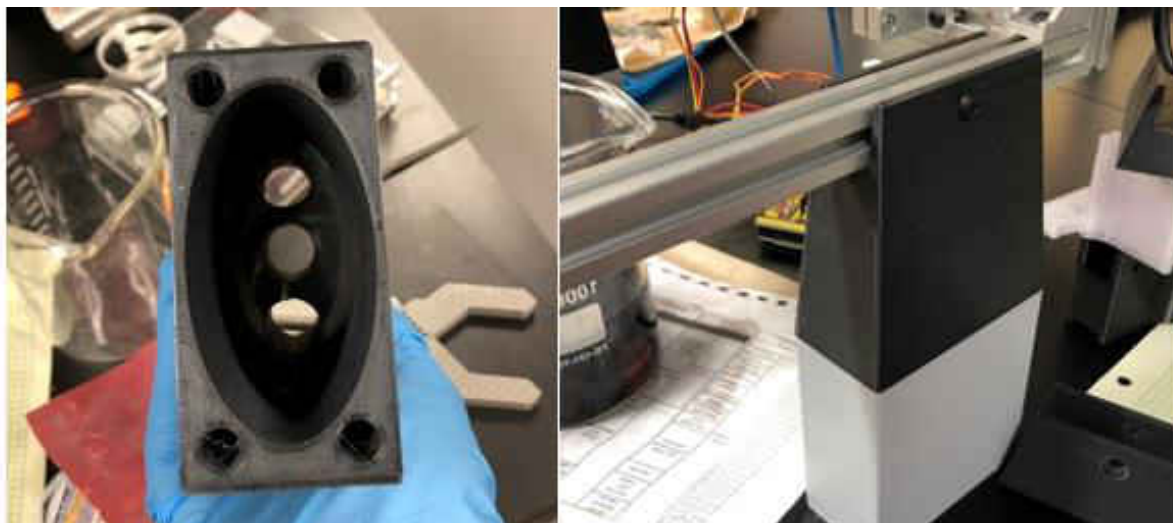


Figure 15. Modular machine feet (black) with added press-fit extensions (gray)

Note that the gray portion of the feet shown to the right is an added extension to expand the overall height of the machine following upscaling the machine to a 10 qt. build volume. The printed feet extensions follow the same geometry with a large elliptical void subtracted through the rectangular block and four additional cylinders subtracted from the bottom. Four cylinders protrude from the top of the feet extensions to lock with a tight clearance fit into the feet attached to the frame. Additional extensions can be attached as they were designed to be stackable, similar to Lego bricks.

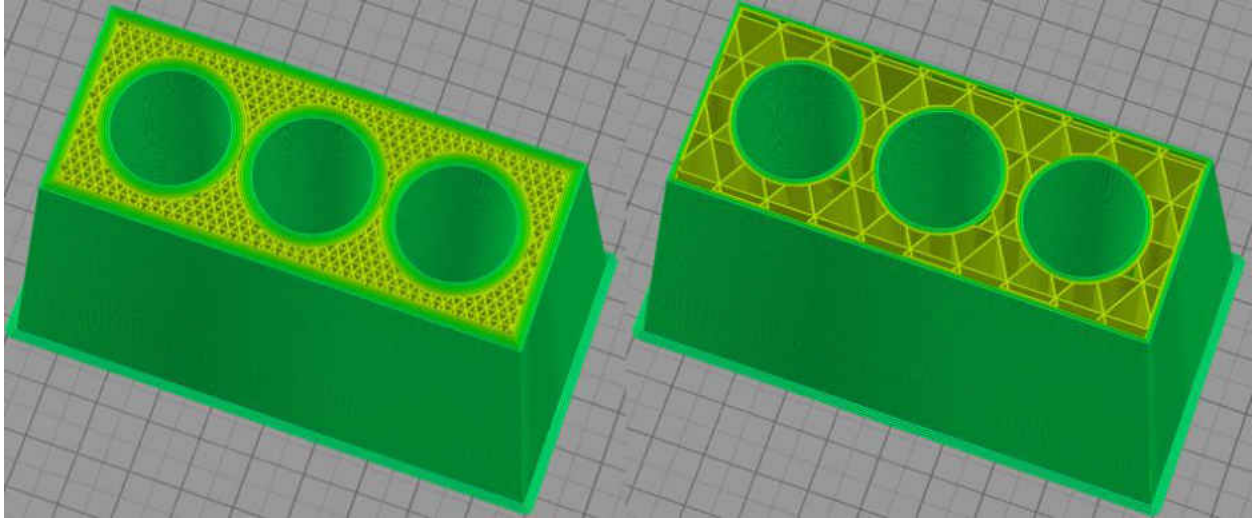


Figure 16. Cross-section view of printer feet prepared for printing with high infill (85%) with 5 perimeter walls (left) and low infill setting (20%) with two perimeter walls

It may seem initially unclear, but previous justifications on material and infill optimization can be applied to optimize part geometry. The printer feet shown in figure 15 and 16 feature circular voids in an otherwise brick-like geometry. The subtraction of these circular geometric features to form empty spaces in the part has no effect on part durability in this special uniaxial compressive loading scenario under the assumption of equivalent mass between optimized and unoptimized parts. That is, removing material in these areas can be thought of as simply moving the volume of material which previously occupied the void to a different area. In a part optimized in this method, the material that would be used as infill is instead used to print the perimeter wall of the void. Increasing the amount of perimeter walls is equivalent to increasing infill under this loading condition.

This optimization yields a decrease in overall print time while part strength and material use remain approximately the same. The difference in print time is difficult to predict as tracing the

path of the toolhead for an entire process is very intensive, in addition to there being limited feedback provided from the machine controller on kinematics.

An in-depth analysis on the kinematics that enables this approach to part optimization is outside the scope of this work. To provide a brief topical explanation, print time can be optimized by reducing the amount of direction changes in a path-based manufacturing process. The infill structure shown in figure 16 requires a path to be routed with sharp direction changes. Rapid changes in direction implicitly slows down the process by forcing the toolhead to accelerate and decelerate more frequently since change in velocity is not instantaneous. Reallocating material from infill to perimeter walls reduces the frequency of sudden changes in direction and will allow the machine to maintain a higher overall print speed. This change in speed is typically not reflected or calculated in software, especially in open source designs as the path routing software is blind to allowable jerk and acceleration rates limited by the machine.

Substrate

The build platform of the machine was the most revised part of the machine. Multiple iterations of the substrate design were required to support changing build volumes and to optimize characteristics of high viscosity fluid flow and optical properties. The entire substrate subassembly of the machine is fully 3D printed except for fasteners. There is little concern for robust design as this component is intended to be treated as disposable and have very short life-cycles.

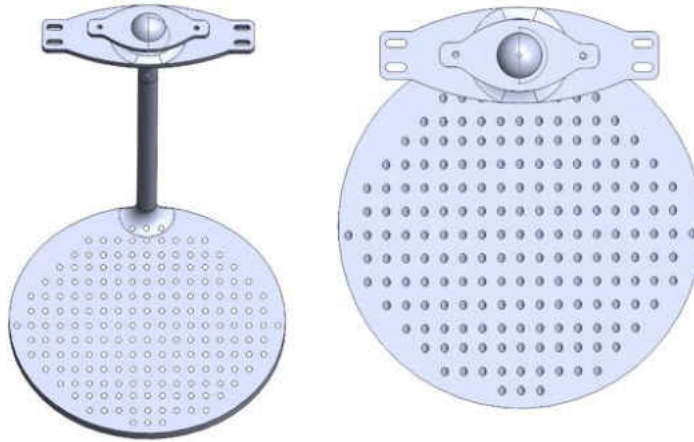


Figure 17. CAD model of final substrate design

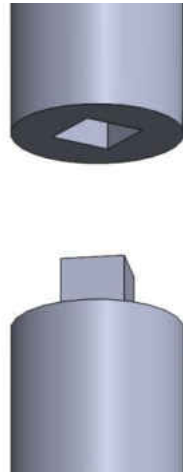


Figure 18. Split portion of shaft

The substrate shown in figure 17 is the entire build platform apparatus, which connects to subframe of the machine responsible for motion along the Z-axis. The build platform (circular portion) was designed perforated at an angle to allow fluid to flow freely through the top and bottom of the platform but prevent light transmission, which may result in material being unintentionally cured below the build surface. The lower portion of the substrate forming the build platform and extending up as part of the shaft. The shaft is separated into two parts as

shown in figure 18, and keyed for alignment and additional surface area for adhesive. J-B Weld epoxy was used to join the two sections of the shaft—the bond strength was ample for the loading required.

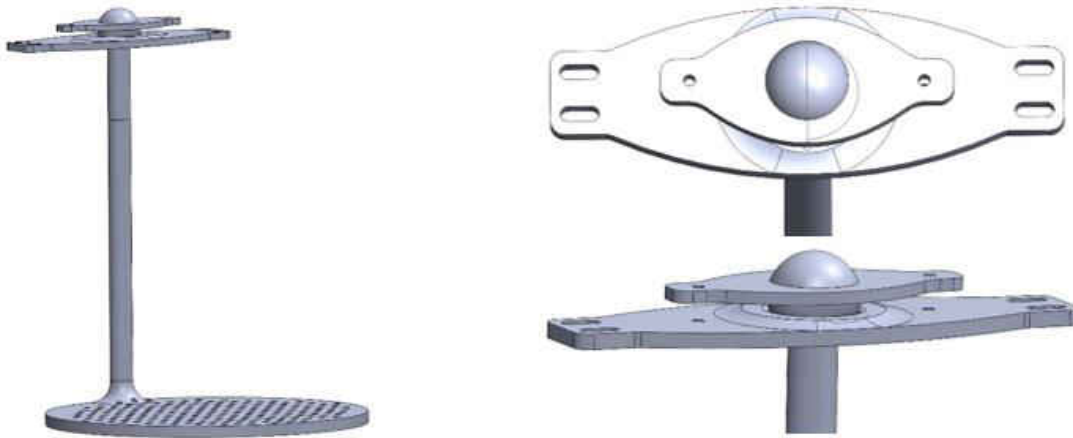


Figure 19. Upper portion of substrate

The shaft was required to be split to accommodate the adjustment mechanism, which features a ball and socket joint with a second parallel plate, which clamps to hold the position of the build platform. The ball and socket mechanism allowed approximately 30° of motion about the mounting point and full rotation. Notable that the mounting plates and upper portion of the shaft were fabricated with PETG plastic for durability and small amount of material flexibility. PLA was favored for rigidity in the lower portion of the shaft and build platform.

Despite the size, the platform does not need to support a significant load should a large portion of the build volume of the machine be utilized. This is an advantage of a top-down SLA configuration; buoyant forces greatly reduce loading on the platform since the part is suspended

in a fluid of nearly identical density. A simple mechanism which can be reproduced daily at low cost while maintaining sufficient rigidity and tolerance of poor precision is highly favorable.

Software

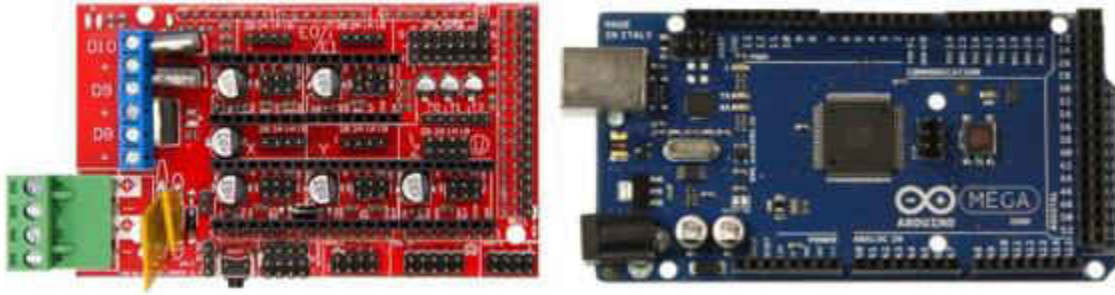


Figure 20. RAMPS 1.4 (left) and Arduino Mega 2560 (right)

The RAMPS (RepRap Arduino Mega Pololu Shield) 1.4 daughterboard was coupled with an Arduino Mega 2560 microprocessor board shown in figure 20. The Arduino board is built around the Atmel ATmega 2560. A single TI-DRV8825 stepper driver was mounted onto the RAMPS 1.4 board and configured for 1/32 microstepping to drive the Z-axis with an 8mm pitch leadscrew coupled to a 1.8° step angle motor. The motor (200 steps/rev) with the selected 8mm pitch leadscrew results in a precision of 400 microns, with 1/32 microstepping yielding a maximum theoretical precision of 12.5 microns.

This configuration is primitive compared to modern machines especially with 32-bit systems becoming more popular and often cheaper, but these controls were chosen for simplicity of configuration. The controls system setup is the most popular open-source choice, offering the largest community support and documentation. Should other students continue the project in this thesis in the future, it will reduce the burden of knowledge and allow for expanded capability

on account of the over-provisioned feature sets. RAMPS boards are typically used to control FDM 3D printers.

The Arduino Mega board is configured with Sprinter firmware. The latest Sprinter commit was dated September of 2013. This is an old firmware chosen intentionally for streamlined configuration as it is stripped down relative to newer firmware by virtue of exclusion of newer features unnecessary for this machine.

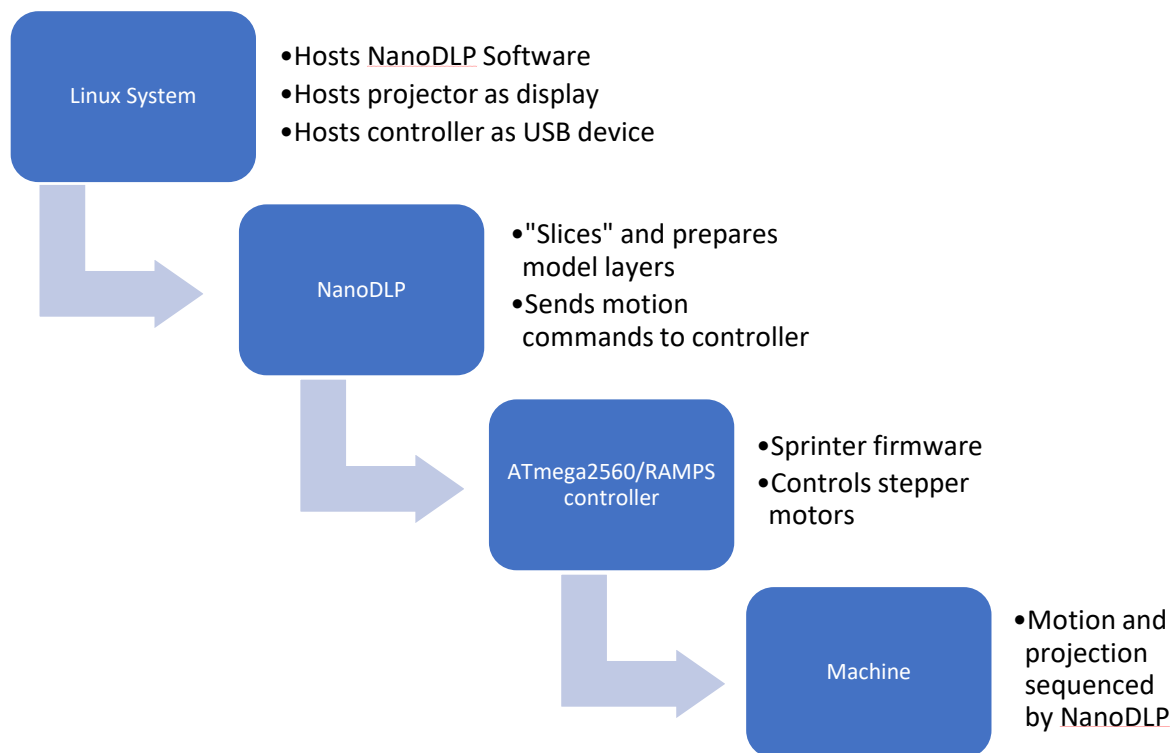


Figure 21. Full system hierarchy

A full diagram of software and hardware coupled workflow is shown in figure 21. This outlines interactions between the host computer and printer microcontroller brokered by NanoDLP software running on the host computer.

NanoDLP was chosen as the slicing software for being open source, available on Linux/Unix based computing systems, and community supported. For FDM processes, slicing consists of partitioning the part into layers of a specified layer height, and then generating a path for the toolhead to extrude filament for each specific layer. DLP SLA is similar in that the part must be partitioned into layers of a specific height, but the slices are flattened into 2D images to be projected onto a liquid resin for UV polymerization.

The projector functions as a secondary display on the host Linux machine. The RAMPS/ATmega board is also connected to the host Linux machine by USB.

Model Preparation

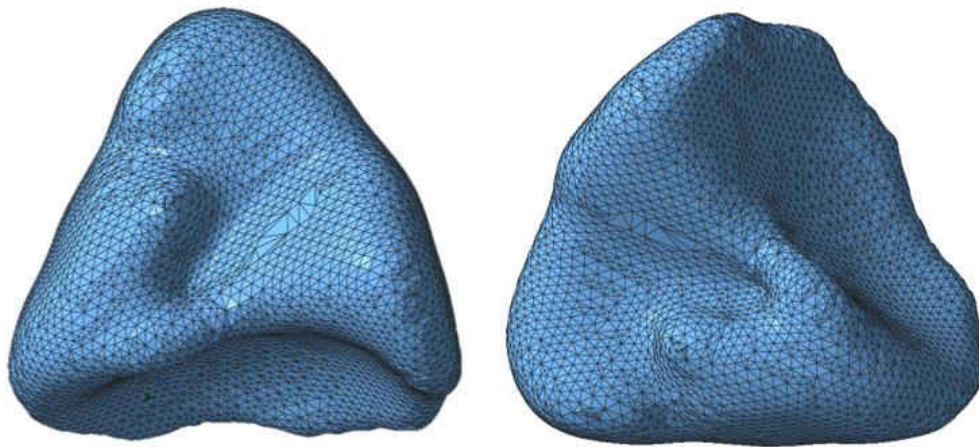


Figure 22. Lung mesh after postprocessing (two perspectives)

Lung meshes as shown in figure 22 were provided by a PhD student working under Dr. Olusegun Illegbusi in cooperation with SegAna. The provided lung meshes were generated in Materialise Mimics software from MRI scan data of a real set of lungs. On appearance the lung meshes seem of acceptable quality but will produce failures when attempting to complete final processing for

any additive manufacturing technique. Meshes generated from Mimics are subject to additional processing by the user to remove artifacts, holes, and add smoothing to the mesh body. It is desirable to apply the least amount of post-processing required to produce a satisfactory mesh since a highly processed mesh will suffer from decreased detail and loss of surface features. Note that the mesh provided is only a surface body and carries no internal detail.

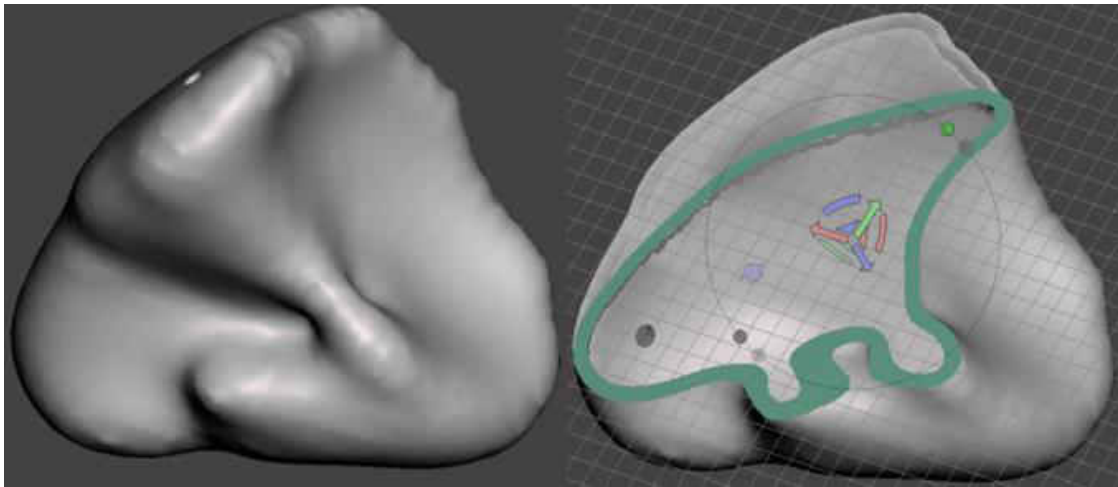


Figure 23. Lung models prepped for printing

The given mesh was initially imported into Autodesk Netfabb, which is a purpose build software for modifying, repairing, and refining mesh bodies. A simple automated repair is performed, which if successful yields a mesh that will be accepted a slicing software.

However, most slicing software will attempt to heal or fill small issues with a selected mesh before slicing. Preparing a mesh for printing beyond a specific slicer software's tolerance will result in a malformed toolset path. Not enough is known about the slicing characteristics of NanoDLP to speculate how poor quality meshes affects output quality. It is speculated that it may be more tolerant of poor mesh quality since the generated layers are flattened into 2D images, but this claim should be taken likely.

The primary issue with faulty meshes is during the hollowing process—this effectively filters poor quality meshes from progressing further in the printing process as a given mesh should be hollowed before attempting to print on an SLA-DLP machine, as shown with green highlighted walls in figure 23. It may be understood, but obviously a non-hollow phantom lung will not function on a respiration apparatus. Following the repair process and prior to hollowing, the mesh was also manipulated in SolidWorks to create a flat surface to use for printing. This is not strictly necessary for a well-developed process and resin system, but use of support material would have complicated attempts to validate the SLA-DLP machine and the UV photopolymer resin used.

The software selected to complete the hollowing process was Autodesk Meshmixer. The software is quite robust and purpose built for handling STL meshes. The print size of the lung model was determined at this stage, as the wall thickness of the part must be specified to generate a hollowed mesh body. As such, the process was repeated when a different sized part was desired instead of simply scaling the part in the slicing software since the slicer will not maintain correct wall dimensions. Drainage holes were also added using Meshmixer. It is necessary to add holes for drainage to allow uncured material to exit the printed body upon completion.

After a mesh has completed post-processing through Netfabb and Meshmixer it can be loaded onto NanoDLP, sliced, and printed.

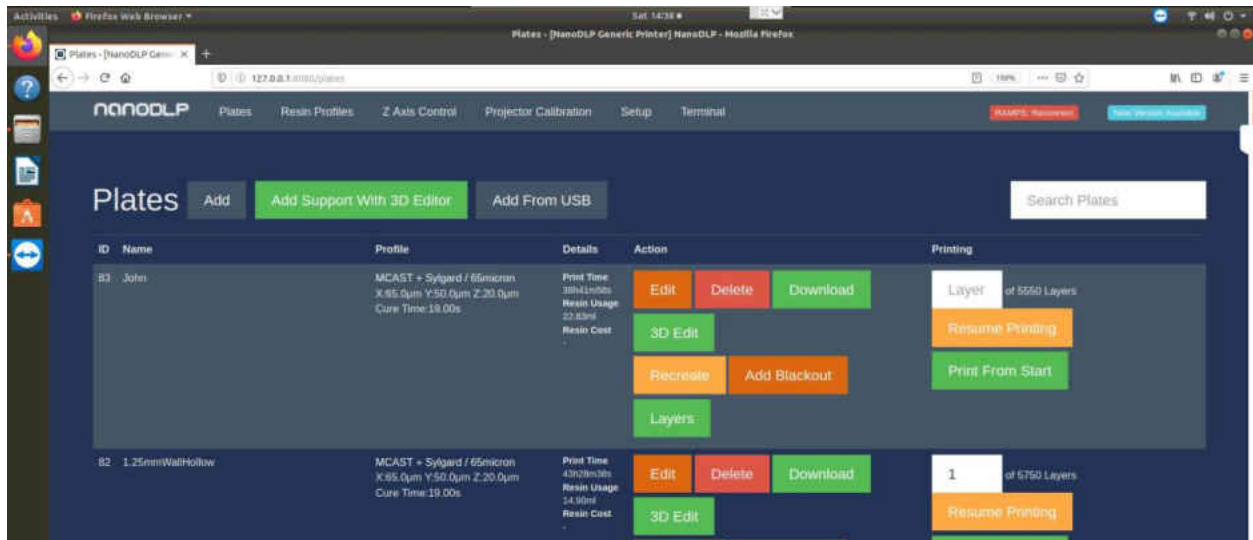


Figure 24. NanoDLP main interface

Figure 24 shows the front page of NanoDLP running in a web browser on an Ubuntu machine. “Plates” refers to a model sliced and prepared for printing. This terminology is used since multiple parts may be loaded onto a single print process. Print time estimation show on the software tend to be approximately 10% quicker than actual elapsed time. Note that the profile names are simply names and do not correspond to actual settings and should be ignored. The software is minimal in terms of features but very lightweight and provides the minimum necessary to properly configure a SLA-DLP printer for high quality part printing.

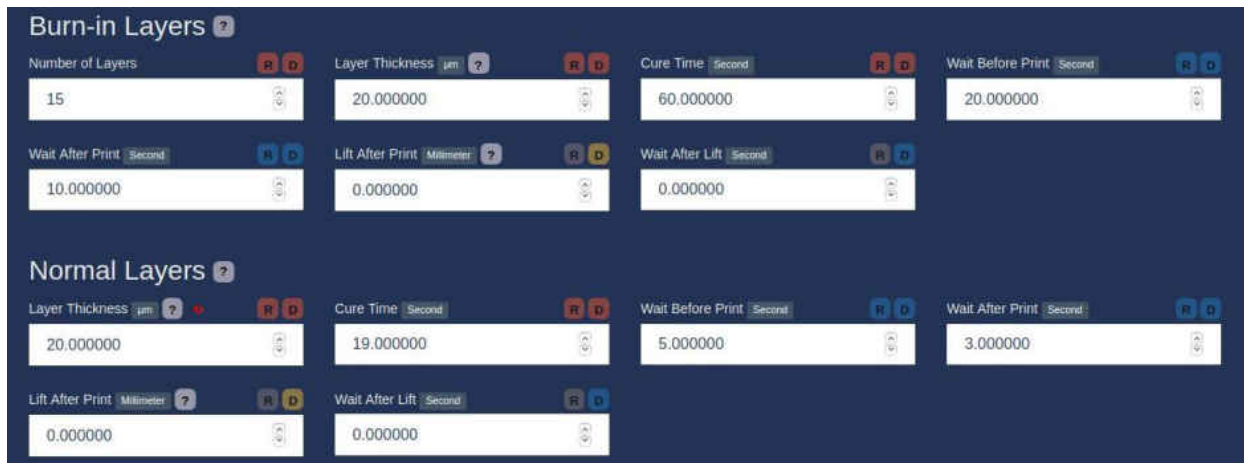


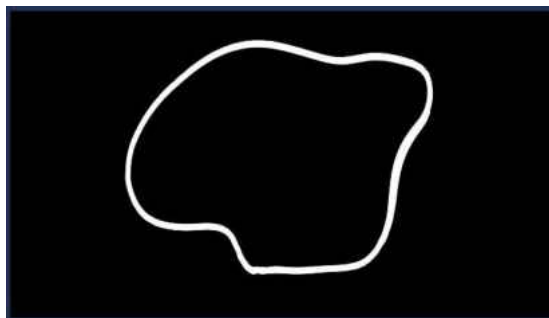
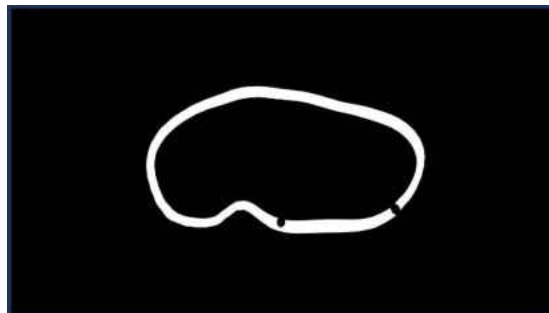
Figure 25. Ultimate print settings used

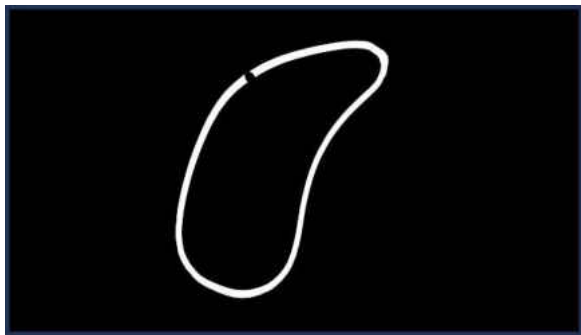
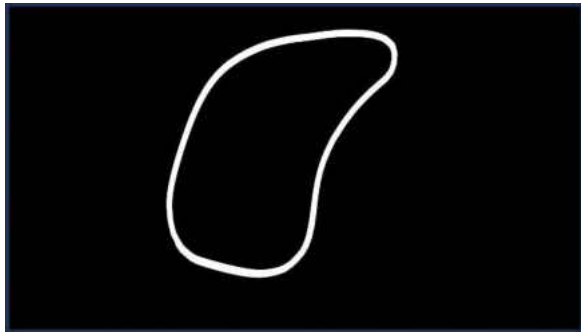
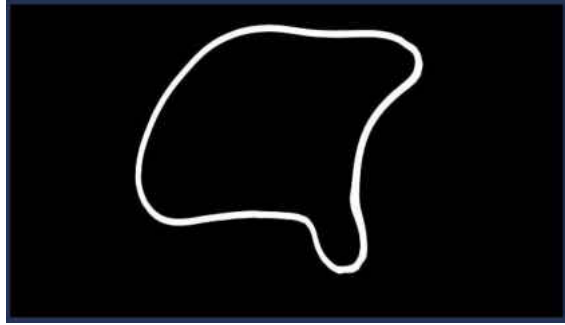
These parameters in the program shown in figure 25 are the primary means to control print quality and machine behavior. These mostly straightforward settings but require extensive experimentation to select proper values when using custom designed polymer resins on a custom built SLA-DLP machine.

In the settings shown in figure 25, the most crucial are *cure time* and *layer thickness*. These are the two primary determinants of print times. This settings configuration is unoptimized and is expected to over-cure the material, as layer times are excessive for layer thickness. Typically increasing layer thickness will increase required cure time, so increasing layer thickness to reduce print time does not yield the same benefit, and it is not as straightforward.

Other settings of interest are the *wait after print* and *wait before print* settings. Increasing these will directly increase intermittent time between layers. Higher values of these are required for larger build volumes and materials with higher viscosity to allow fluid to flow and settle after the substrate is moved along the Z-axis upon completing a layer.

The following image sequence is provided to conclude the chapter and is a sample output of a few select slices from a lung phantom part prepared in NanoDLP. The white regions of the slices are projected onto the surface of the vat containing the liquid UV curable photopolymer resin. 9 sample layer slices of the approximate 6000 layer slices were selected sequentially at periodic points in the print.





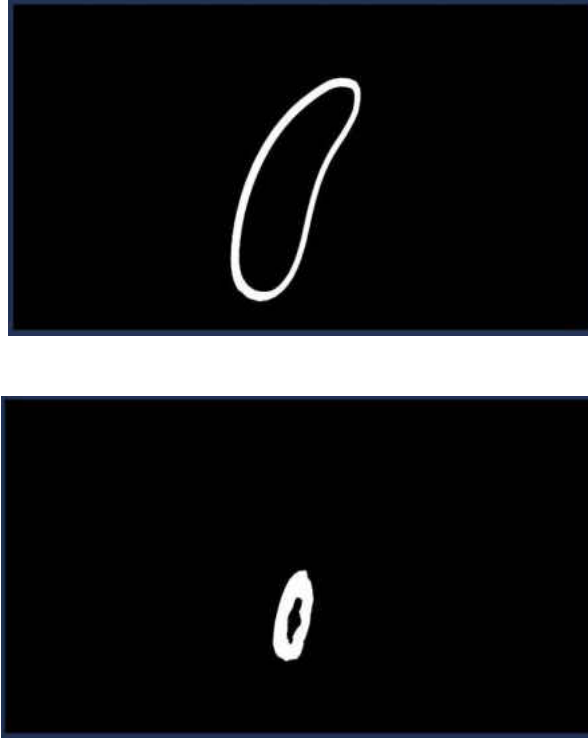


Figure 26. Collective figure of 9 discrete sequenced slices intended for SLA-DLP printing of a lung phantom

TESTING AND EVALUATION

Early Stage Testing

Physical machine mechanics were simple, requiring motion in only one dimension. Early stage testing as previously detailed in the material formulation section of the methodology chapter was performed before the inception of this thesis. 20x40x100mm test strips were produced with the intent to perform tensile testing on the samples. The 20x40x100mm strips were produced using PLA 3D printed molds and cured with an off-shelf UV light source. Early testing with this method was intended to determine successful percent by weight photoinitiator content required to complete polymerization as well as the maximum reactive diluent concentration before failure to complete polymerization. These samples were qualified by inspection on pass or fail basis.

As described in in table 1, after finding a critical ratio of 9 parts reactive diluent to 1 part crosslinking oligomer, iterative testing was returned to a composition of 8:2 parts of the respective epoxy resin components. The 8:2 reactive diluent to crosslinking oligomer composition was used beyond that point and non-rigorous tensile testing was performed to estimate usability of this composition.

A 20x40x100mm test strip was manufactured using a 3D printed mold and tensile testing was performed using an MTS Systems universal testing machine. The tensile tests were performed with the assistance the Structures and Materials Design lab directed by Dr. Kawai Kwok. The material was found to exhibit a modulus of elasticity of approximately 300 kPa and the data was used to evaluate feasibility of the material composition for use to produce 3D printed lung phantoms. The modulus of elasticity (approximately 300 kPa) was predicted to be sufficient to

meet the needs of the project. Note that an elastic modulus of approximately 300 kPa is cited in this section and in the following figures, which is in direct conflict of the elastic modulus value quoted as approximately 350 kPa in the rest of this body of work. This discrepancy is explained in the immediate content following.

The tensile tests were performed before the inception of this body of work, and the data was not preserved as it was intended to quickly validate the material composition. Material properties did not need to be an exact match with lung tissue, but the elastic modulus needed to be low enough to be practical and usable in a respirator apparatus. The same composition was ultimately successful in tidal breathing motion simulation in a respirator apparatus, so this conjecture was eventually shown to be correct.

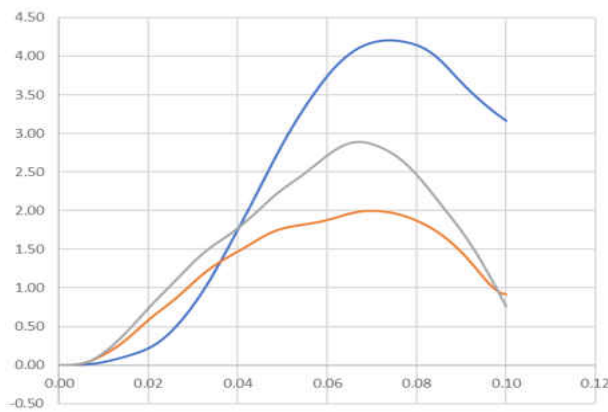


Figure 27. Deformation simulation strain response of real lung tissue (15 kPa)

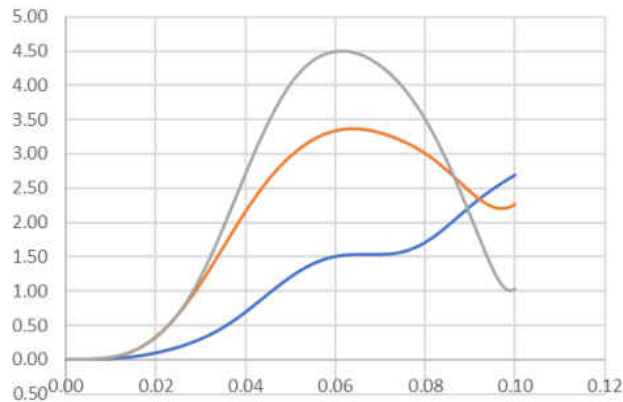


Figure 28. Deformation simulation strain response of elastomer photopolymer formulation 5 of table 1 (300 kPa)

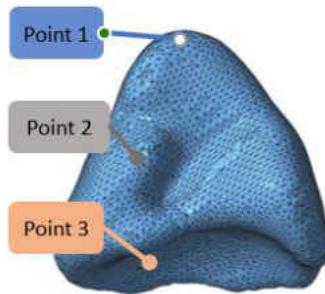


Figure 29. Provided legend for figures 27 and 28. Points 1, 2, 3, correspond to the top surface, inner surface near hilum, and bottom surface, respectively

Strain response plots shown in figure 27 and 28 were provided by Dr. Olusegun Ilegbusi's now graduated former PhD student Don Nadun Kuruppumullage [11]. These plots should not be held to a rigorous academic standard and were used as a last resort. The original creator should not be held accountable for the information shown in these plots, as they were not intended to be used in this capacity. Additional testing to obtain more robust data sets was scheduled for the graduating semester and submission of this body of work; however the material required to conduct tensile testing arrived briefly before non-essential activities at University of Central Florida were halted for the sake of public health on account of the COVID-19 pandemic. Hence a

conservative estimate of 350 kPa was reported as the modulus of elasticity. Extrapolation from the findings of Patel et al. and first-hand testing experience can assert an approximation of 350 kPa with high confidence.

Useful information can still be ascertained from the plots in figures 27 and 28. Stress as a function of strain rate shown in figures 27 and 28 are shown to be mostly linear up to approximately 0.06 strain. As per sponsor requirements, strain rates up to 0.1 only were required as pertinent to human lungs. This suggests that the UV photocurable elastomer resin system developed for 3D printing is sufficient at low strain rates but may need additional model adjustment for higher strain simulations. Utilizing infill structures to approach this issue is discussed further in the future works section.

Machine Print Testing



Figure 30. First successfully 3D printed material sample

The first sample produced shown in figure 30 was printed on a bottom-up laser based SLA machine (Peopoly Moai). An extruded 2D shape was chosen for initial test samples. A significant

amount of time and resources was required to meet this milestone due to the sheer amount of unknown parameters when working undocumented material. The material used in figure 30 is the 8:2 reactive diluent to crosslinking oligomer polymer resin represented as 5th composition in table 1 under the material formulation section of the methodology chapter. This part was close to the elastic limit of the bottom-up SLA printing process.

The elastic limit is an implicit limitation on print height when using bottom-up SLA machines with elastic materials. This can be explained by defining characteristics of this type of machine.

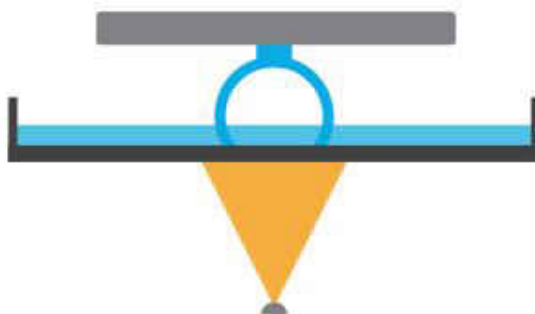


Figure 31. Diagram of bottom-up SLA machine

The substrate of a bottom-up SLA machine similar to the diagram shown in figure 31 relies on a PDMS (Polydimethylsiloxane) layer. The PDMS layer serves as a cushion to accommodate for slight height variation across the build platform, but also serves as a material resistant to cured UV photopolymer resin adhesion. That is, for this machine to function a thin layer of material is sandwiched and cured between the build platform and previous cured layers of the part—the thickness of this layer is determined by the selected printing layer height. Bottom-up SLA machines have a “peel” motion where the platform is raised an extra amount of distance to detach the cured layer from the PDMS lining the build substrate. Beyond a certain point, the

allowable deflection of the printed part exceeds the distance of the peel motion of the machine, causing the part to become stuck in the same position for the following layer.

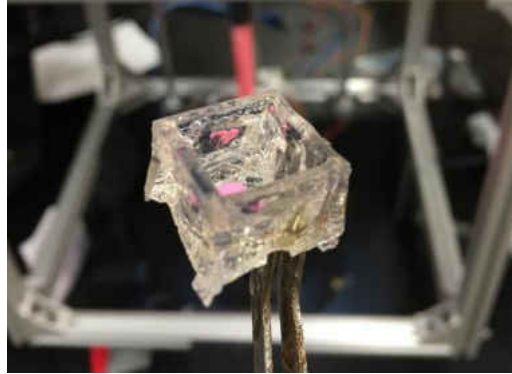


Figure 32. First SLA-DLP 3D printed sample

The first sample printed on the top-down SLA-DLP machine is shown in figure 32. The part chosen was a hollow cube with one face removed to eliminate overhangs (i.e. unsupported structures). A 1L beaker was used as the vat with a PLA printed substrate sized to fit into the beaker. Glycerin suspension was not needed at this point.



Figure 33. Late (left) vs early (right) print iteration samples

A small toy dinosaur was chosen as the consistent reference part for iterative improvement of the printing process. The part was chosen for the ease in vertical scaling while still maintaining a variety of features that can be inspected for print quality. The most important feature of the model being the spines of the body with gaps between them. Poorly controlled UV light sources and lack of photoinhibitors will cause unintentional curing in these gaps, as shown by the early print sample depicted on the right of figure 33. Prints of the same part later in the process development cycle with the addition of Mazyo OB+ photoinhibitor allows formation of sharp and highly detailed spines, such as depicted on the left of figure 33.



Figure 34. Original model of part shown in figure 33.

The original model shown in figure 33 is provided in figure 34 for the sake of context. Note that the feet and arms of the model also contain sharp features and overhangs. Quality of these portions can also be inspected to gauge control over the UV source.



Figure 35. Final testing print at large volume

Upon upscaling the machine to a 10 qt. build vat, a large version of the toy dinosaur was successfully printed and was observed to feature sharp detail across spine area while also maintaining satisfactory overhang performance near the arms and feet, shown in figure 27. Overhang performance in this regard refers to how effectively depth of polymerization is controlled. Poor polymerization control results in excess material cured below the region of the overhang, as UV light is absorbed below the intended region causing unwanted excess polymerization.

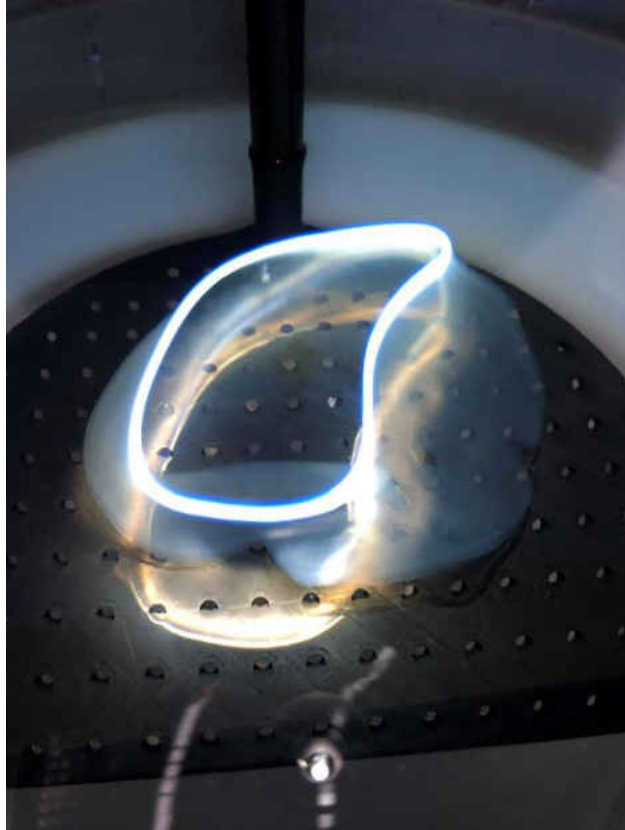


Figure 36. Late iteration lung phantom being printed

A lung phantom in the middle of an SLA-DLP printing process is shown in figure 36. The bright white outline is light projected onto the surface while the semi-transparent body is visible below the surface. When the UV source is inactive the part will appear fully transparent in the vat. Additionally, refraction distorts the apparent depth of the body which makes gauging progress and size visually slightly misleading. Figure 37 displays three perspectives of the ultimate part produced.



Figure 37. Final lung phantom print using custom resin formulation on custom designed SLA-DLP machine

Manufacturing Challenges

One of the more problematic underlying issues with the developed process is the liquid glycerin addition used to suspend the liquid photopolymer resin. An implicit challenge with floating a liquid resin on top of glycerin arises from the buoyant force generated when the part is submerged into the glycerin region of the vat. Buoyant force acting on the body of the submerged part during the printing process will cause deflection and slightly distort the shape of the body during printing on account of the low modulus of elasticity—this would not be an issue for a non-flexible liquid photopolymer resin. Deflections may become significant enough to cause critical misalignment with subsequent layers and becomes increasingly probable the physically larger the model being printed is. This was the suspected reason for a noticeable loss in print quality when printing large lung phantom bodies compared to reference parts. Attempts to decrease the effective stiffness of printed lung phantoms by reducing wall thickness were also suspected to fail because of buoyant forces.

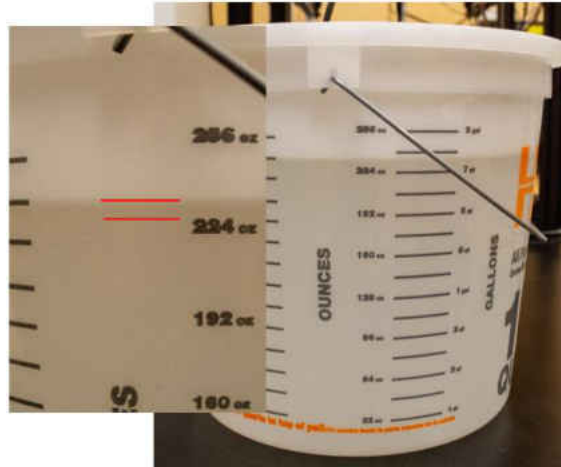


Figure 38. 10 qt. vat with suspended custom developed UV photopolymer resin suspended, marked in red

A mostly filled 10 qt. pail used as a resin vat is shown in figure 38. The red lines in figure 38 mark the thin region of the custom liquid UV photopolymer. The remaining liquid in the vat is liquid glycerin.

A less obvious issue that constrained lung phantom printing was the physical geometry of the lung. Many organic structures, such as human lungs, do not contain convenient geometric features for determining part orientation. This can be accommodated for by slightly modifying one surface of the lung to allow it to be oriented onto the print platform. The more pressing complication with organic geometry is concave inward geometric features with respect to the build platform.

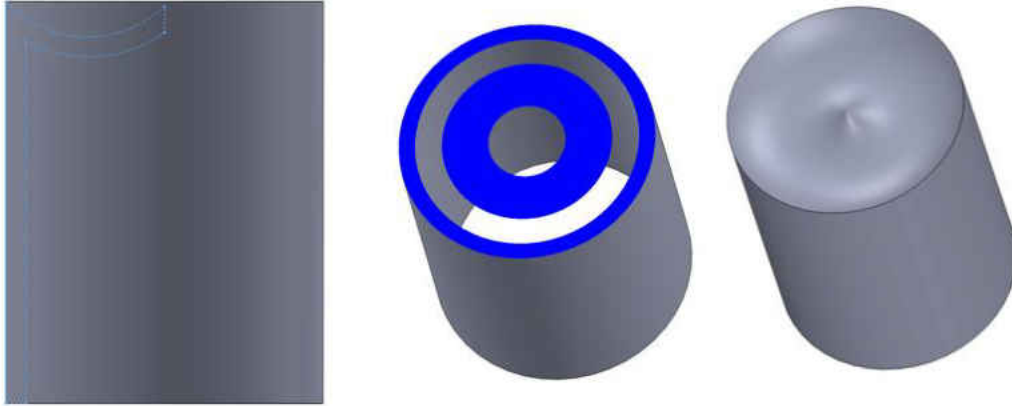


Figure 39. Sample part with concave geometry

To better clarify the issue, a concave inward part was drafted for the sake of demonstration shown in figure 39. The feature across the top surface is similar to wave formation following a drop of water into another liquid. This type of feature has sections where there is discontinuous geometric features (highlighted in blue). Note that below the blue highlighted region there is no material present for the layer to connect to. This results in an “island” formation in the sequence of layers when slicing for SLA-DLP 3D printing. This part would not be printable unless an internal structure is added, or the part is reoriented to avoid this feature. In printing of lung phantoms, this reduces the amount of options to orient the part for printing. In production of the lung phantom, a region of concave island geometry was flattened and used as the surface to be oriented onto the print substrate.

CONCLUSION AND FUTURE WORK

In Summary of Work Completed

This thesis covered a successful project on full process development for producing a SLA-DLP 3D printed highly elastic lung phantom. A cost efficient, modular, rapidly deployable, and easily scalable machine was developed for printing UV photopolymer resins. Machine print parameters were configured iteratively until satisfactory print quality was met using a known good formulation of the custom designed UV resin.

3D meshes of lungs were provided by a former student from an adjacent project. Meshes were generated from MRI data and converted into 3D mesh models in Materialize Mimics software by the former student. The mesh model was received and refined with additional post-processing to obtain a mesh of sufficient quality to be prepared for SLA-DLP 3D printing.

A UV curable liquid resin photopolymer system was formulated through iteration and testing to yield a photopolymer resin that was successfully printed in a custom purpose-built SLA-DLP 3D printer. Initial iterations were performed on a bottom-up laser SLA machine until satisfactory polymerization of the material was met. Initial print settings before iteration on bottom-up laser SLA machine were based off known good settings for an off-shelf reference acrylate UV photopolymer resin intended for use in bottom-up laser SLA machines. The combination of the machine and custom resin formulation were observed to yield acceptable print quality for the purpose of validation in early stage research and development. The custom UV photopolymer resin mixture was observed to exhibit a Young's elastic modulus of approximately 350 kPa.

The custom UV photopolymer resin was ultimately suspended on liquid glycerin inside a 10 qt. vat functioning as the build chamber. Resin suspension on glycerin was found to be an incredibly effective means for optimizing the process since mixing, purchasing, and handling large volumes of designed photopolymer is resource and labor intensive. Addition of glycerin in the vat as an inert fluid enables a small fractional volume of liquid photopolymer resin to be functionally equivalent to a large volume of liquid. However, there are suspected drawbacks to utilizing a floating resin system—particularly due to buoyant effects from the differences in density between cured polymer material and glycerin. This is a highly specific fringe case scenario as ultra-flexible 3D printing dependent on liquid material suspension in a top-down SLA configuration is not common.

The printed lung phantom was affixed into a respirator apparatus provided by SegAna and was able to simulate tidal breathing motion successfully for the extent of the length that was tested. Approximately 3 minutes of tidal motion was simulated using the lung phantom without issue.

[Future Work](#)

There remains much to be developed forking from the content of this thesis. The machine, software and processing, and material have extensive capacity for improvement.

[Machine Design](#)

Many components on the machine, such as the ball and joint pressure mount which fixes the build substrate in place was designed for low cost rapid production. The design met the specific needs of this project but is too flimsy and inconsistent as it relies on the operator to properly level the platform without guidance.

The build substrate should be manufactured with a different material as well. The design is acceptable, however FDM printed parts are porous and have textured surface finishes. This surface finish caused excessive adhesion of cured material on the print substrate. A suggested stopgap solution was to modify the substrate to feature a build surface of polystyrene.

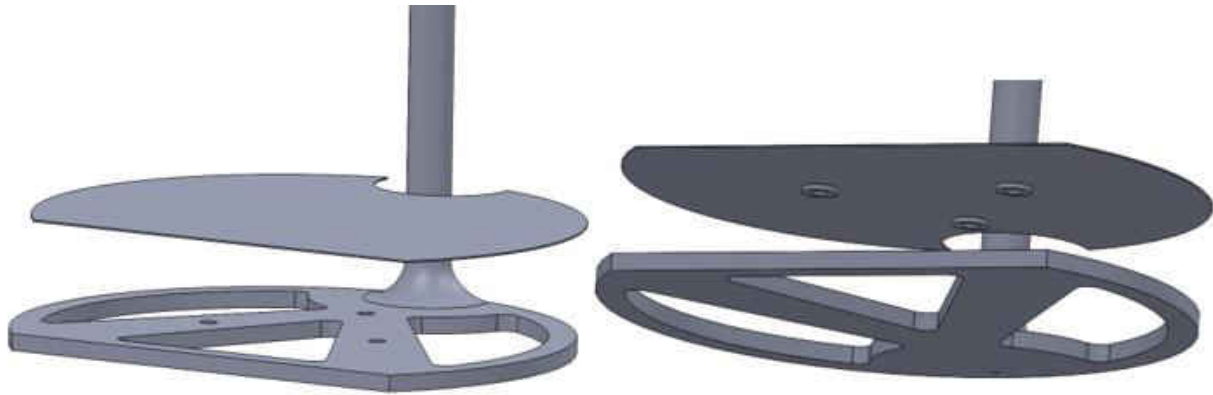


Figure 40. Alternate dissolvable platform

The modified platform shown in figure 40 uses a thin printed polystyrene surface attached to a printed PLA frame with 3 press-fit neodymium magnets. The surface is slightly elevated from the mounting platform to preserve fluid flow. Polystyrene is dissolvable in natural solvent D-limonene which would eliminate the need to peel the printed part from the build substrate. This was a proposed solution that was not tested. It is unknown how the cured UV photopolymer will react to submersion in the selected solvent.

Software and Processing

Open source printing software and tools to support top-down SLA processes with elastomers are severely underdeveloped as there is little commercial space for it since the specific niche is already occupied by large additive manufacturing companies such as 3D Systems. Furthermore, technical knowledge requirements and high setup costs for SLA-DLP 3D printers are barriers of

entry for hobbyists who will typically be better served by more traditionally cost-effective bottom-up style SLA machines.

There also does not exist a ubiquitous and accessible piece of software to assign variable infills in structures to modify deformation characteristics. Adding a variable infill structure will allow the strain response of a 3D printed elastomer lung phantom to be modified to closer match the strain response of a real lung and improve accuracy of patient specific simulated tidal motion.

An additional body of work was completed on the topic of modeling and manually inserting a specific type of infill as adjacent work evaluating ANSYS SpaceClaim and SolidWorks as a solution for custom infill structures. Findings suggested that traditional parametric CAD will certainly be an ineffective solution and concludes by suggesting other modeling automation tools such as OpenSCAD.



Figure 41. ML optimized cast provided by Stratasys

The best feasible solution is likely an ML (machine learning) approach to mapping unique and specific strain responses by augmenting mesh models with machine generated infill structures. Figure 40 is an FDM printed cast demoed at a Stratasys seminar in March of 2018; this part is optimized for material efficiency by selectively reinforcing areas on the cast that are subject to high loading conditions—effectively creating a part with controlled and variable stress and strain response. While Stratasys’ developments are closed source, it demonstrates that a viable solution can be built with machine learning. Areas of a printed part will need to be reinforced internally to reduce strain response in order to serve the requirements of an elastomer lung phantom with patient specific deformation characteristics.

Material Design

There is additional potential for the material formulation to be optimized. As per Autodesk’s open source resin formulation, it is likely that the quantity of photoinitiator added can be reduced, in addition to the quantity of photoinhibitor slightly increased. Excess photoinitiator increases sensitivity to unintended curing of excess material below the intended region of polymerization. Increased photoinhibitor will help control unintended curing of the same type by reducing sensitivity in lower regions of the vat.

Most importantly, it should be possible to slightly increase the reactive diluent to crosslinking oligomer ratio to above 8:2 and below 9:1. Increasing parts reactive diluent will reduce the amount of crosslinking which will reduce the elastic modulus of the material.

It should also be considered that there are a vast amount of printing parameters that can be varied in addition to material formulations.

REFERENCES

- [1] Oh S, Kim S. Deformable image registration in radiation therapy. *Radiation Oncology Journal*. 2017;35(2):101–111. doi:10.3857/roj.2017.00325
- [2] Ilegbusi OJ, Li Z, Seyfi B, et al. Modeling Airflow Using Subject-Specific 4DCT-Based Deformable Volumetric Lung Models. *Int J Biomed Imaging*. 2012;2012:350853. doi:10.1155/2012/350853
- [3] Ilegbusi O., et. al. Final Comprehensive Report. Deformable Lung Phantom. University of Central Florida. 2014.
- [4] W. Xin, "Development of Radiology Lung Phantom with 3D Foam Printing," PowerPoint, UCF, 2018.
- [5] Patel, Dr. Dinesh & Sakhaei, Amir Hosein & Layani, Michael & Zhang, Biao & Ge, Qi & Magdassi, Shlomo. (2017). Highly Stretchable and UV Curable Elastomers for Digital Light Processing Based 3D Printing. *Advanced Materials*. 29. 1606000. 10.1002/adma.201606000.
- [6] E. Wilhelm, *Autodesk Standard Clear Resin Is Now Open Source*, ember-autodesk-1545937.hs-sites.com/blog/open-source-resin, 2015.
- [7] UVP Inc., 1986. Apparatus For Production Of Three-Dimension Objects By Stereolithography. 4575330.
- [8] T. Ebihara, N. Venkatesan, R. Tanaka, and M. S. Ludwig, "Changes in Extracellular Matrix and Tissue Viscoelasticity in Bleomycin–induced Lung Fibrosis: Temporal Aspects," *American journal of respiratory and critical care medicine*, vol. 162, pp. 1569-1576, 2000.

[9] F. Liu, B. S. Shea, J. D. Mih, A. M. Tager, and D. J. Tschumperlin, "Lung parenchymal tissue stiffness in fibrosis and cellular responses to substrate stiffness," *Biophysical Journal*, vol. 96, p. 395a, 2009

[10] B. Rundlett, "Photoinitiator Selection," DSM Functional Materials, PowerPoint, *Radtech Technology Conference*, 2012.

[11] N. Kuruppumullage, "Finite Element Modeling of Lung Phantom Using Elastomer as Material," PowerPoint, *UCF*, 2018.